学位論文
Doctoral Thesis

Nephric duct lineage-specific role of non-muscle myosin II in mouse kidney development

(マウス腎臓発生における非筋肉型ミオシン II の腎管系譜特異的な役割の検討)

ハキュー ファヒム　カビール
Fahim Kabir Monjurul Haque

熊本大学大学院医学教育部博士課程医学専攻
HIGO プログラム 4 年コース

指導教員

西中村 隆一 教授
熊本大学大学院医学教育部博士課程医学専攻腎臓発生学

2017 年　9 月

学　位　論　文

Doctoral Thesis

Title of Thesis: **Nephric duct lineage-specific role of non-muscle myosin II in mouse kidney development**

論文題名 ：マウス腎臓発生における非筋肉型ミオシン II の腎管系譜特異的な役割の検討

著 者 名: ハキュー ファヒム　カビール

Name of Author: Fahim Kabir Monjurul Haque

指導教員名 ：熊本大学大学院医学教育部博士課程医学専攻腎臓発生学　西中村 隆一 教授
Name of supervisor:

審査委員名　:
Name of examiner

脳発生学担当教授　　嶋村　健児

腎臓内科学担当教授　　向山　政志

形態構築学担当教授　　福田　孝一

泌尿器科学担当教授　　神波　大己

２０１７年 ９月

Table of Contents

(All praise and thanks to Allah for his guidance and who has taught me all that I know and I am)

Acknowledgements

I would like to express my gratitude to my supervisor Prof. Ryuichi Nishinakamura. He has been very supportive of my work and encouraging throughout my PhD tenure. He has guided me immensely throughout my work and life.

I would also like to express my gratitude to Yusuke Kaku, Sayoko Fujimura, Tomoko Ohmori, Robert S. Adelstein, and Shunsuke Tanigawa for their technical support and advice.

I also want to thank all members of the Department of Kidney Development at Kumamoto University for always being there for me.

I would also like to acknowledge the support of the HIGO program for my PhD scholarship.

Last but not the least, I would like to acknowledge my immense gratitude and love to my parents, family, and friends.

Abstract

Background and purpose: During kidney development, formation of the functional urinary exit tract depends on correct sprouting of the ureteric bud (UB) from the nephric duct (ND). In these morphogenetic processes, the roles of Ret signaling are well established. However, the regulatory roles of intracellular cytoskeletal proteins remain unclear. In this project, I have studied the role of two non-muscle myosin heavy chains, IIA and IIB, by deleting both *Myh9* and *Myh10* genes encoding these proteins from ND/UB lineage cells in mice.

Methods: *Myh9/Myh10* were deleted from ND/UB lineages by crossing $Myh9^{flox/flox}Myh10^{flox/flox}$ mice with *Hoxb7Cre* mice. They were analyzed at birth and various embryonic days (E), including E10.5, E11.5, and E14.5, by histology (section immunofluorescence staining and *in situ* hybridization as well as whole mount immunostaining).

Results: Deletion of *Myh9/Myh10* from ND/UB lineages in mice resulted in hydronephrosis/hydroureter at birth due to misconnection/physical blockade between the ureter and bladder. This hydronephrosis/hydroureter was likely to happen because of basally protruding epithelial cells and thus formation of ectopic UB at mid-gestation. Moreover, apical constriction and E-cadherin-mediated intercellular adhesions were reduced in the epithelia, which likely caused the apical extrusion of cells into the lumen followed by massive luminal apoptosis. Genetic suppression of tyrosine kinase receptor (*Ret*) did not rescue these phenotypes, which indicates involvement of a Ret-independent pathway. However, mutant cells exhibited hyperactivation of extracellular signal-regulated kinase (ERK). In vitro culture of mutant kidney rudiments in the presence of an ERK inhibitor partially ameliorated the phenotypes, thus indicating the involvement of Ret-independent mechanisms.

Conclusion: In developing kidneys, non-muscle myosin II is essential for maintenance of the apicobasal integrity of renal epithelia.

List of Reference Articles

Fahim Haque, Yusuke Kaku, Sayoko Fujimura, Tomoko Ohmori, Robert S. Adelstein, Ryuichi Nishinakamura.
Non-muscle myosin II deletion in the developing kidney causes ureter-bladder misconnection and apical extrusion of the nephric duct lineage epithelia
Developmental Biology. 427, 121-130, 2017. http://dx.doi.org/10.1016/j.ydbio.2017.04.020

List of Abbreviations

ND	Nephric duct
UB	Ureteric bud
E	Embryonic day
CND	Common nephric duct
NMHC	Non-muscle myosin heavy chain

1. Background

1.1 Mouse kidney and urinary exit tract development

The origin of the mammalian kidney is intermediate mesoderm. In mice, kidney development begins upon formation of the pronephric duct. The pronephric duct arises from the anterior intermediate mesoderm at embryonic day (E) 8.5 and then elongates caudally to form the nephric duct (ND). Between E9.5 and E10.5, the ND reaches toward the cloaca and merges with it. Concomitantly, at around E10.5, the ureteric bud (UB) sprouts from the ND and metanephric mesenchyme arises from posterior intermediate mesoderm cells present in the nephrogenic cord. The UB continues to elongate and invades the metanephric mesenchyme by E11.5 (Short and Smith, 2016; Chia et al., 2011) (Figure 1). The kidney develops through reciprocal induction between these two precursor tissues: the UB and metanephric mesenchyme. The UB induces the mesenchyme to differentiate into nephron epithelia, thus forming the upper part of the nephron (glomeruli and renal tubules). During this time, the UB continues to branch extensively and gives rise to a tree-like structure consisting of collecting ducts and ureters, thus forming the urinary exit tract.

The formation of a functional urinary exit tract depends on sprouting of the UB from the correct position of the ND. The initial site of UB sprouting and its further branching patterns are strictly controlled and mainly regulated by glial cell line-derived neurotrophic factor (GDNF)-Ret signaling (Costantini and Kopan, 2010). The metanephric mesenchyme secretes GDNF that acts on the Ret tyrosine kinase receptor of the epithelia on the ND/UB. In the UB, Ret activates phosphorylation of kinases including extracellular signal-regulated kinase (ERK). In addition, Ret signaling stimulates many downstream target genes such as *Etv4/5*, *Wnt11*, and *Ret* itself (Lu et al., 2009). GDNF-Ret signaling forms two feed forward loops between the metanephric mesenchyme and UB, where Ret upregulates the expression of *Ret* itself and *Wnt11* in the UB (Pepicelli et al., 1997). Simultaneously, Wnt11 signals toward the metanephric mesenchyme to upregulate the expression of GDNF (Majumdar et al., 2003). In addition, movements of the cells in the ND, which lead to UB formation, are promoted by the GDNF-Ret signaling (Chi et al., 2009). A negative feedback loop of GDNF-Ret signaling is also regulated by *Ret*. *Ret* upregulates Spry1 and Robo2 that act as negative regulators of GDNF-Ret signaling. Deficiency of the downstream target genes of GDNF-Ret signaling has been reported to affect kidney development. Deficiency of *Ret* or *Gdnf* causes a reduction in UB branching and eventually kidney agenesis (Costantini and Kopan, 2010; Durbec et al.,

1996). Mice lacking both *Etv4* and *Etv5* have complete failure of kidney development. Furthermore, mice lacking both *Etv4* and one allele of *Etv5* develop renal agenesis or severe hypodysplasia (Lu et al., 2009). Mutation in *Wnt11* causes defects in UB branching morphogenesis and kidney hypoplasia (Majumdar et al., 2003). Conversely, deletion of negative regulators of GDNF-Ret signaling, Robo2 and *Spry1* (Basson et al., 2005; Grieshammer et al., 2004), or hyperactivation of *Ret* by a mutation (Hoshi et al., 2012) causes hyperactivation of ERK, positional shifting of the sprouting site of the UB, and ectopic UB budding. Such aberrant UB budding can eventually lead to improper connection formation between the ureter and bladder. In normal kidney development between E11.5 and E13.5, the common nephric duct (CND), which is the caudal segment of the ND to the UB sprouting site, undergoes physiological apoptosis, and eventually the distal end of the UB forms a direct connection with the bladder (Figure 1) (Mendelsohn, 2009; Chia et al, 2011; Stewart and Bouchard, 2014). Any impairment of this process can lead to misconnection of the ureter and bladder. The disorders described above, which occur because of *Ret* hyperactivation, can cause this impairment that eventually leads to hydroureter and hydronephrosis, i.e. dilation of the ureter and kidney, respectively (Basson et al., 2005; Grieshammer et al., 2004; Hoshi et al., 2012).

While the roles of Ret signaling are well established in UB sprouting from the ND and subsequent branching, the regulatory roles of intracellular cytoskeletal proteins in the morphogenetic processes remain unclear.

1.2 Non-muscle myosin II in maintaining cell-cell adhesion and polarity

The cytoskeletal protein non-muscle myosin II belongs to the class II myosins and is abundantly expressed throughout animal body. It is a motor protein involved in various cellular properties including cell shape and cell adhesion during development and in the adult organism. Non-muscle myosin II modulates cell adhesion and polarity together with actin filaments (Conti and Adelstein, 2008; Smutny et al., 2010). At adherens junctions, actomyosin anchors cadherins via β and α catenins. These adherens junctions and subsequently formed tight junctions establish epithelial apicobasal polarity by separating the apical and basal domains of epithelia. Actomyosin also regulates epithelial attachment to the basement membrane through interactions with integrins which are receptors for the extracellular matrix (Conti and Adelstein, 2008).

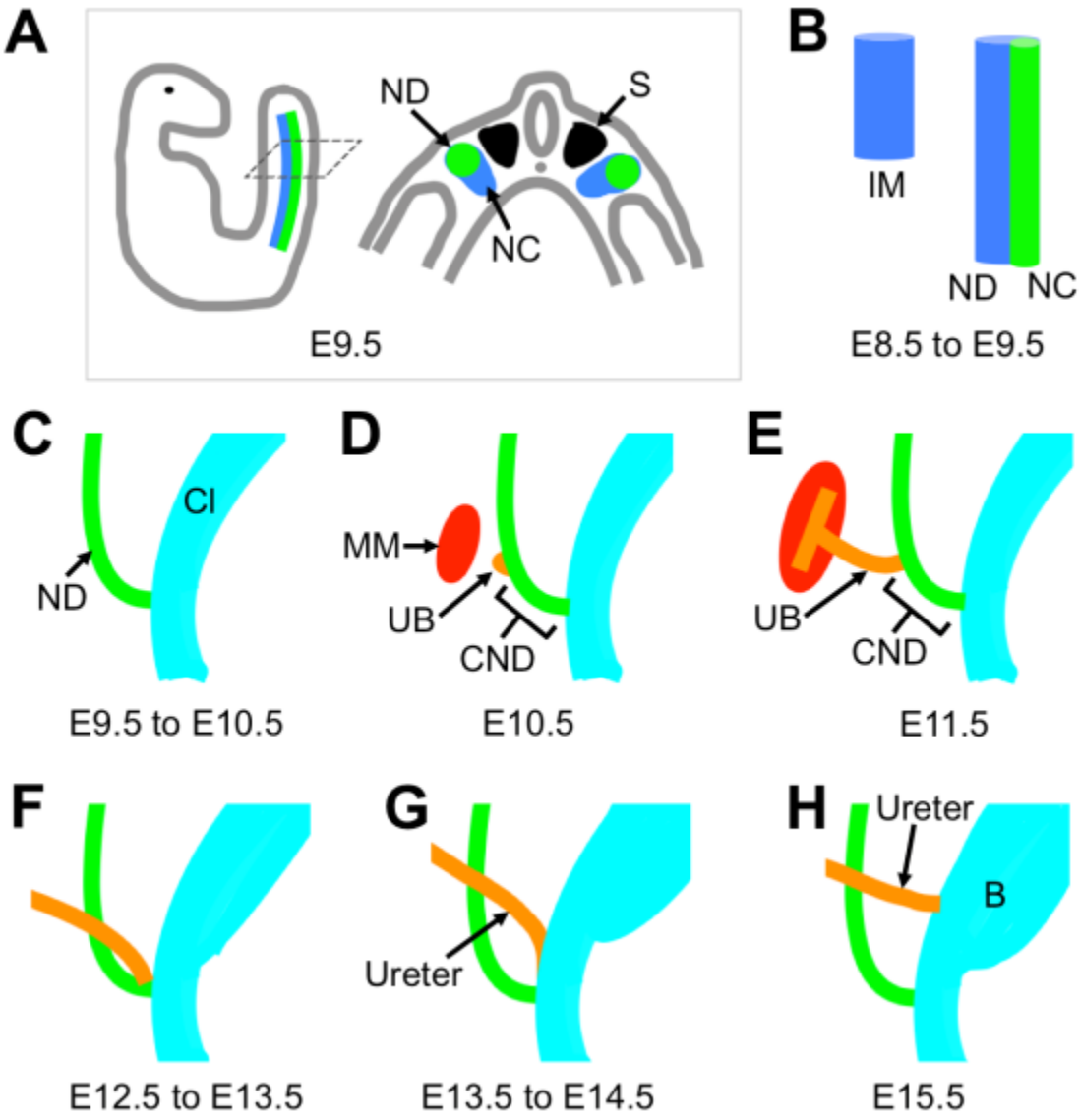

Figure 1: Development of the urinary exit track. (A) Diagram of the E9.5 embryo (left panel) and schematic cross-section showing the nephric duct (ND, green), nephrogenic cord (NC, green), and somite (S). (B) ND arises from the intermediate mesoderm (IM) at around E8.5 and elongates caudally. (C) Between E9.5 and E10.5, the ND reaches toward the cloaca and merges with it. (D) At around E10.5, the ureteric bud (UB) sprouts from the ND and elongates. Simultaneously, metanephric mesenchyme (MM) arises from posterior mesoderm cells. (E) By E11.5, the UB invades the MM and forms a T-shape bifurcation upon branching. The caudal segment of the ND to the UB sprouting site is the common nephric duct (CND). (F) Between E11.5 and E13.5, the CND undergoes physiological apoptosis, and the distal end of the UB merges with the cloaca. (G, H) Between E13.5 and E15.5, the ureter aligns; the most caudal part of the ureter undergoes apoptosis, and eventually the mature ureter-bladder connection forms.

1.3 Non-muscle myosin II in vertebrates and mouse kidney development

In vertebrates, there are three isoforms of non-muscle myosin heavy chains (NMHCs), IIA, IIB, and IIC, which are widely disturbed throughout organisms. These isoforms are encoded by three genes, *Myh9*, *Myh10*, and *Myh14*, respectively (Conti and Adelstein, 2008).

Mutations in *Myh9* cause infantile disorders in humans, such as Fechtner and Epstein syndromes, which are characterized by platelet and kidney abnormalities (Kelley et al., 2000; Sekine et al., 2010; The May-Hegglin/Fechtner Syndrome Consortium, 2000).

Deficiency of *Myh9* in mice causes loss of cell adhesion in visceral endoderm during the peri-implantation period, and deficiency of *Myh10* causes heart and brain defects during mid-gestation (Conti et al., 2004; Tullio et al., 1997). Because mice lacking *Myh14* alone do not have any abnormal phenotypes (Ma et al., 2010), *Myh9* and *Myh10* might play predominant roles in embryonic development compared with *Myh14*. In mouse kidney development, *Myh9* and *Myh10* encode the major myosin II proteins (Recuenco et al., 2014). While *Myh9* deletion in metanephric mesenchyme causes tubular dilatation leading to renal failure at the adult stage, deletion of both *Myh9* and *Myh10* affects nascent nephron formation resulting in perinatal death, which suggests that these genes have redundant roles in metanephric mesenchyme (Recuenco et al., 2014). During mouse kidney development, both NMHC IIA (encoded by *Myh9*) and NMHC IIB (encoded by *Myh10*) are expressed ubiquitously, including expression in the ND and UB epithelia. However, it has been already reported that deletion of only *Myh9* from the ND/UB lineage does not cause apparent kidney defects (Recuenco et al., 2014).

2. Objective of the study

The objective was to examine the tissue-specific role of non-muscle myosin heavy chains IIA and IIB by deleting *Myh9* and *Myh10* from ND/UB lineage cells in the developing kidneys of mice. The results revealed unexpected phenotypes that demonstrate the important roles of non-muscle myosin II in this lineage *in vivo*.

3 Methods

3.1 Generation of mutant mice

Myh9$^{flox/flox}$ and *Myh10*$^{flox/flox}$ mice (MMRRC #32096 and #16981, respectively) have been described elsewhere (Jacobelli et al., 2010; Ma et al., 2009). The *Hoxb7Cre* mouse strain was obtained from the Jackson Laboratory (Yu et al., 2002). The *RetCreER* mouse strain (Chi et al., 2009; Uesaka et al., 2013), which was used for genetic crosses to generate *Ret* heterozygosity without tamoxifen treatment, was kindly provided by Dr. Hideki Enomoto at Kobe University, Japan (deposited as CDB0518K, http://www2.clst.riken.jp/arg/mutant%20mice%20list.html). These mouse strains were backcrossed to the C57BL/6 mouse strain for at least three generations. The following primers were used for genotyping: Hoxb7Cre-F2 (5′-TGGGCCGGGGTCACGTGGTCAGA-3′) and Hoxb7Cre-R2 (5′-CGACGATGAAGCATGTTAGCTG-3′) for the *Hoxb7Cre* allele (500 bp); hER-1 (5′-TGGAGATCTTCGACATGCTG-3′) and hER-2 (5′-GCCATCAGGTGGATCAAAGT-3′) for the *RetCreER* allele (209 bp). The primer sequences for *Myh9* and *Myh10* alleles as well as PCR conditions have been described previously (Recuenco et al., 2014). Blood urea nitrogen, creatinine, and albumin levels in serum samples were analyzed by standard methods using ultraviolet light, hydroxyl triiodobenzoic acid, and bromocresol green, respectively. All animal experiments were approved by the Animal Care and Use Committee of Kumamoto University (#A27-018) and performed in accordance with the institutional guidelines of Kumamoto University.

3.2 Section immunostaining

Mouse embryos or kidneys were fixed with 10% formalin or 4% paraformaldehyde, and embedded in paraffin or OCT compound, respectively. Immunostaining was carried out using a BlueMap Kit and automated Discovery System (Roche) or manually for immunofluorescence staining. The following primary antibodies were used: anti-Myh9 (HPA001644; Sigma); LTL (B1325; Vector Laboratories); anti-Wt1 (sc192; Santa Cruz Biotechnology); anti-cytokeratin (c2562; Sigma); anti-cleaved caspase-3 (9661; Cell Signaling Technology); anti-p-aPKC (ab62372; Abcam); anti-pHH3 (06-570; Millipore); anti-E-cadherin (610181; BD Transduction Laboratories); anti-pERK (4370; Cell Signaling Technology); anti-fibronectin (ab2413; Abcam); anti-Pax2 (901001; Biolegend). Immunofluorescence was visualized with an LSM780 confocal microscope (Zeiss). Seven

mutant and seven control embryos were analyzed at E11.5, and four mutant and four control embryos were analyzed at E10.5 with consistent results.

In some experiments, an ImmPress Reagent Kit (MP-7401 or MP-7402; Vector Laboratories) and Alexa Fluor tyramide (T20948; Thermo Fisher Scientific) were used to enhance signals or perform double staining with antibodies from the same host species. Sections were incubated with primary antibodies and anti-rabbit or anti-mouse secondary antibodies conjugated with peroxidase polymers, according to the manufacturers' instructions. The sections were then incubated with Alexa Fluor tyramide diluted in amplification buffer containing hydrogen peroxidase for 15 min at room temperature. Subsequently, the sections were subjected to a second round of staining in a standard manner. The following primary antibodies were used: anti-Myh10 (DSHB, CH11 23-5; Developmental Studies Hybridoma Bank) in Fig. 1; anti-YAP (sc101199; Santa Cruz Biotechnology) and anti-Yap/Taz (8418; Cell Signaling Technology) in Fig. S3; anti-pERK (4370; Cell Signaling Technology) in Fig. 6C, the latter of which allowed triple staining of pERK (rabbit), Myh9 (rabbit), and E-cadherin (mouse) with minimal cross-reactivity. The specificities of the anti-Yap and anti-Yap/Taz antibodies have been demonstrated previously in *Yap*-null and *Yap/Taz*-null mutant mice, respectively (Reginensi et al., 2015).

3.3 Whole mount immunostaining

Immunostaining of dissected or cultured tissues was carried out as described previously (Hoshi et al., 2012). Briefly, tissues were fixed with 4% paraformaldehyde for 30 min at 4°C, washed with PBS-Tr (0.3% Triton X-100 in PBS), blocked with PBS-BB (1% bovine serum albumin, 0.2% dry skim milk, and 0.3% Triton X-100 in PBS) overnight at 4°C, and then incubated with anti-Pax2/E-cadherin primary antibodies diluted in PBS-BB overnight at 4°C. After washing with PBS-Tr, the samples were incubated with Alexa Fluor-conjugated secondary antibodies diluted in PBS-BB overnight at 4°C, followed by washing with PBS-Tr. Some of the stained samples were cleared with SeeDB (Ke et al., 2013) for better visualization and then embedded in agarose. Immunofluorescence was visualized with an SZX16 stereo microscope (Olympus). Six kidneys from control mice and 10 kidneys from mutant mice were analyzed with consistent results.

3.4 Organ culture

Kidney tissues were dissected from E10.75 mice (tail somite numbers: 35–40) and cultured in Dulbecco's modified Eagle's medium (DMEM)/F12 (Thermo Fisher Scientific)

containing 10% serum on Transwell filters (0.4 μm; Corning) (Hoshi et al., 2012)(Kaku et al., 2013). Left and right kidneys were cultured separately, one in the presence of ERK inhibitor U0126 (3 μM; Sigma) and the other in the presence of the vehicle (dimethyl sulfoxide; DMSO). The concentration of U0126 was optimized using wild-type embryos. After 48 h of culture, the specimens were subjected to whole mount immunostaining for Pax2 and E-cadherin. Three independent experiments were performed, and representative data are shown.

3.5 *In situ* hybridization

In situ hybridization of 10% formalin-fixed paraffin-embedded sections was performed as described previously (Kaku et al., 2013) using an automated Discovery System (Roche) equipped with an OmniMap anti-rabbit HRP Amplification HQ Kit, Anti-HQ Alkaline Phosphatase Multimer Kit, or ChromoMap Blue Kit (all from Roche), according to the manufacturer's protocols. The probes for *Ret*, *Wnt11*, and *Etv4* were cloned by PCR and labeled with digoxigenin using RNA polymerase.

3.6 Madin-Darby canine kidney (MDCK) cell culture

MDCK cells were cultured on collagen-coated plates as described previously (Hogan et al., 2009). Briefly, type IA collagen was prepared according to the manufacturer's protocol (Collagen Gel Culture Kit; Nitta Gelatin), and each well of a 12-well plate was coated with 0.6 ml collagen. Cells were seeded at a density of 5×10^5 cells/well and cultured in DMEM containing 10% serum. At confluency, the cells were treated with 50 or 100 μM blebbistatin (Wako) for short periods (5 or 10 min). Total cell lysates were prepared using NuPAGE LDS sample buffer (Thermo Fisher). Western blotting was performed as described previously (Tanigawa et al., 2015). The following primary antibodies were used: anti-pERK (4370; Cell Signaling Technology) and anti-β-actin (3700; Cell Signaling Technology). The experiments were repeated three times with consistent results. Images were acquired and quantified by densitometry using ImageJ software (Schneider et al., 2012). After measuring the band intensities, relative intensities were calculated and normalized to the intensities of β-actin (loading control). Statistical analysis was performed by the Student's *t*-test.

3.7 Statistical analyses

Six fields in stained sections (two fields/section for three mice) were used to count $pHH3^+$/E-$cadherin^+$ cells in both control and *Myh9/Myh10* mutant mice. The percentage of $pHH3^+$/E-$cadherin^+$ cells in each field was calculated and analyzed by the Student's *t*-test.

Data are presented as the mean ± standard deviation. The percentages of $Casp3^+$/$E\text{-}cadherin^+$ and $pERK^+$/$E\text{-}cadherin^+$ cells were calculated and analyzed in a similar manner.

4 Results

4.1 Non-muscle myosin IIA and IIB are abundantly expressed in kidney epithelia

During mouse kidney development, both NMHC IIA (encoded by *Myh9*) and NMHC IIB (encoded by *Myh10*) were expressed ubiquitously, including expression in the ND and UB epithelia (Figure 2)

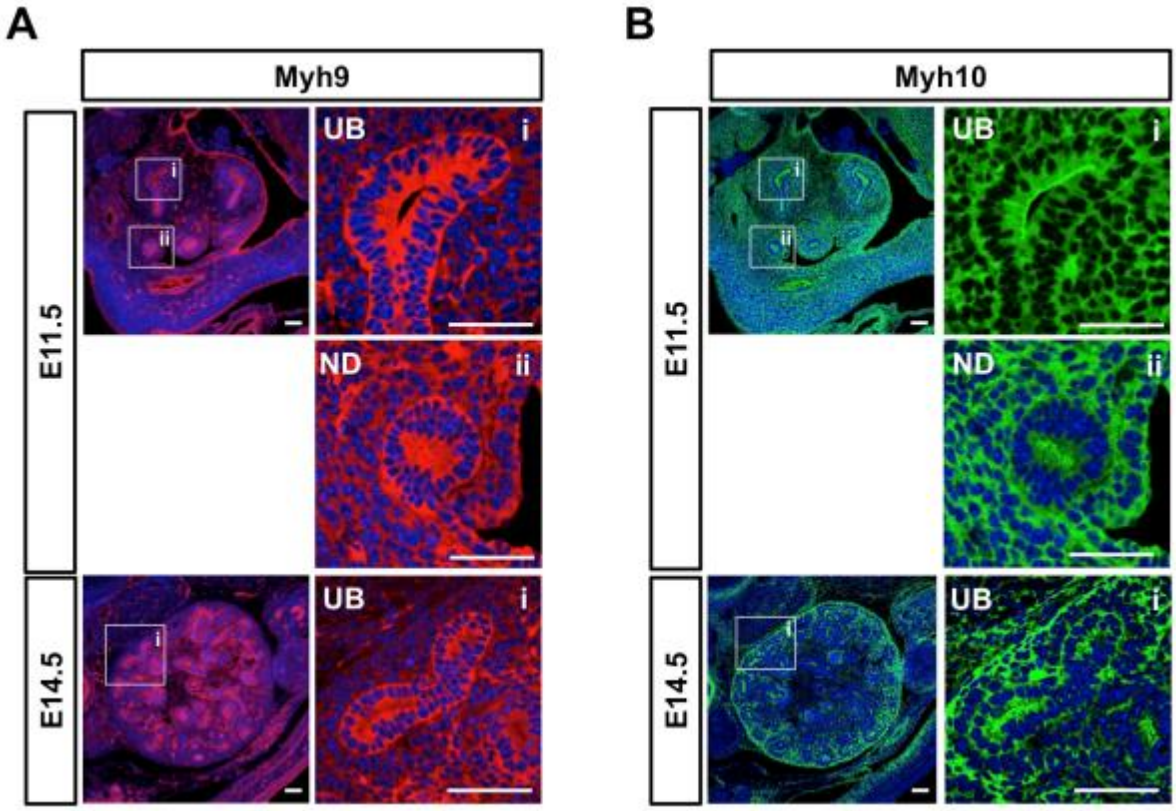

Figure 2: Both NMHC IIA (*Myh9*) and NMHC IIB (*Myh10*) are ubiquitously expressed in the kidney epithelia. (A and B) Expression Myh9 (red) and Myh10 (green) in the ND and UB epithelia at E11.5 and E14.5. Scale bars: 50 µm

4.2 Specific deletion of *Myh10* from ND/UB lineages causes no defects in kidney development

Both alleles of *Myh10* were deleted in ND/UB lineages by crossing the floxed allele of *Myh10* with the *Hoxb7Cre* mouse strain expressing Cre recombinase specifically in ND/UB lineages. Myh10 disappeared only in E-cadherin+ ND/UB epithelia, indicating successful deletion of *Myh10* (Figure 3A). However, some cells retained *Myh10* because of the mosaic Cre activity of the *Hoxb7Cre* mouse strain (Figure 3A). The mutant mice showed no obvious defects in their kidney morphology that was analyzed by hematoxylin and eosin (HE) staining (Figure 3B). Both control and mutant mice had similar patterns of UBs, glomeruli, and proximal tubules that were visualized by immunostaining for respective markers, cytokeratin (UB marker), Wt1 (glomerular marker), and LTL (proximal tubule marker) (Figure 3B). Renal functions were also similar between control and mutant mice. The levels of blood urea nitrogen, creatinine, and albumin in sera from 13-week-old mice did not differ significantly between the two groups (Figure 3C). Thus, deleting only one of the two genes in ND/UB lineages did not affect kidney development.

4.3 ND/UB lineage-specific *Myh9/Myh10* deletion causes hydroureter/hydronephrosis at birth

Because mice lacking *Myh9* or *Myh10* in ND/UD lineages did not have any apparent kidney defects, mice lacking both *Myh9* and *Myh10* in ND/UB lineages were generated. The double-mutant mice (*Hoxb7Cre; Myh9*$^{flox/flox}$ *Myh10*$^{flox/flox}$) were born, but many of them showed hydroureter and/or hydronephrosis (Figure 4A and 4B).

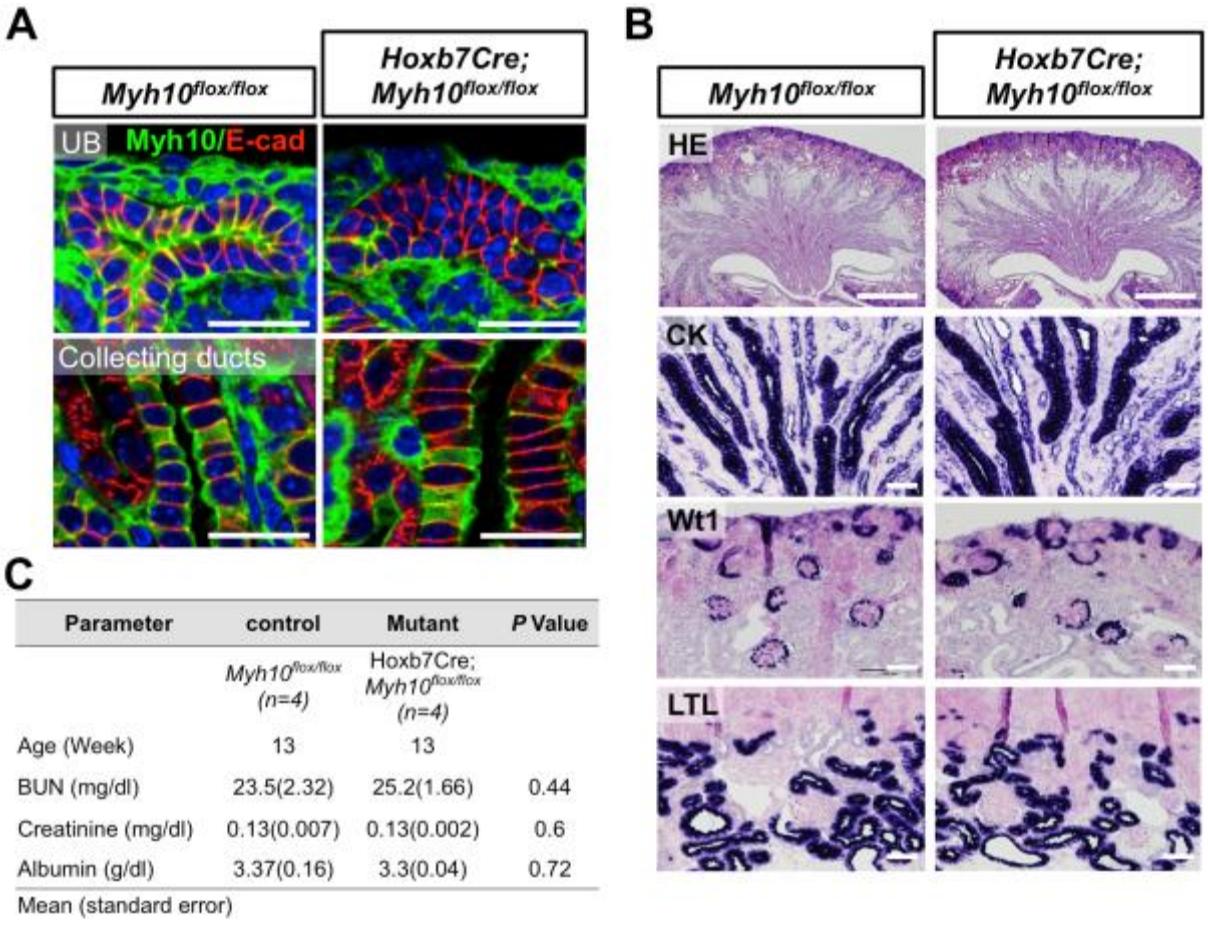

C

Parameter	control	Mutant	*P* Value
	Myh10$^{flox/flox}$ *(n=4)*	Hoxb7Cre; *Myh10*$^{flox/flox}$ *(n=4)*	
Age (Week)	13	13	
BUN (mg/dl)	23.5(2.32)	25.2(1.66)	0.44
Creatinine (mg/dl)	0.13(0.007)	0.13(0.002)	0.6
Albumin (g/dl)	3.37(0.16)	3.3(0.04)	0.72

Mean (standard error)

Figure 3: ND/UB lineage-specific deletion of *Myh10* causes no abnormal phenotypes. (A) Immunostaining of Myh10 in control kidney (left column) and ND/UB-specific *Myh10* mutant kidney (right column) sections at birth. Myh10 was absent in E-cadherin^{+} mutant epithelia. The presence of Myh10 expression in some of the mutant epithelia indicated the mosaic Cre activity of *Hoxb7Cre* mice. (B) Histological analysis of control kidneys (left column) and ND/UB-specific *Myh10* mutant kidneys (right column) at birth. From top to bottom rows: HE staining and immunostaining of cytokeratin (CK), Wt1 (glomerular marker), and LTL (proximal tubule marker). Dark purple indicates a positive signal. Sections were counterstained with nuclear fast red. (C) Levels of blood urea nitrogen (BUN), creatinine, and albumin in sera from 13-week-old mice showed no significant differences between control and ND/UB-specific *Myh10* mutant mice. Scale bars: 25μm in A; 500 μm in the first row of B; 50 μm in the second, third and fifth rows of B.

A

	Hydroureter & Hydronephrosis	Hydronephrosis	Hydroureter	Normal
Control	0/28 (0%)	0/28 (0%)	0/28 (0%)	28/28 (100%)
Mutant	10/22 (45.5%)	2/22 (9%)	1/22 (4.5%)	9/22 (41%)

B

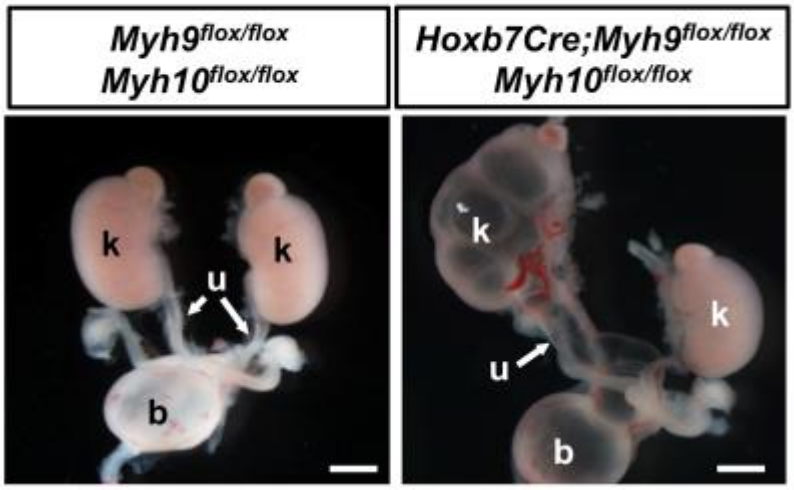

Figure 4: ND/UB lineage-specific *Myh9/Myh10* deletion causes hydroureter/hydronephrosis at birth. (A) Frequencies of ND/UB-specific *Myh9/Myh10* mutant kidneys with hydronephrosis and/or hydroureter at birth. (B) Hydronephrosis and hydroureter in a newborn *Myh9/Myh10* mutant mouse. Abbreviations: b: bladder; k: kidney; u: ureter. Sale bars: 1 mm.

4.4 ND/UB lineage-specific *Myh9/Myh10* deletion causes misconnection between the ureter and bladder at birth and leads to hydronephrosis/hydroureter

To investigate the cause of the hydronephrosis/hydroureter, an ink injection experiment was performed in newborn mouse kidneys, revealing that the ink injected into the mutant renal pelvis did not flow into the urinary bladder (Figure 5A). This result indicated the presence of a physical blockade or misconnection between the ureter and bladder. Furthermore, while examination of serial sections revealed a ureter opening into the bladder in control mice, a ureter opening was not detected in mutant mice (Figure 5B). This

blockade/misconnection prevented urine from flowing through the ureter to the bladder, which eventually resulted in hydroureter and hydronephrosis. In severe cases (four of 22 examined ureters), dilated ureters were blind-ended and completely detached from the urinary bladder (Figure 5C). Thus, deletion of both *Myh9* and *Myh10* caused misconnection of the ureter and bladder, resulting in hydroureter/hydronephrosis.

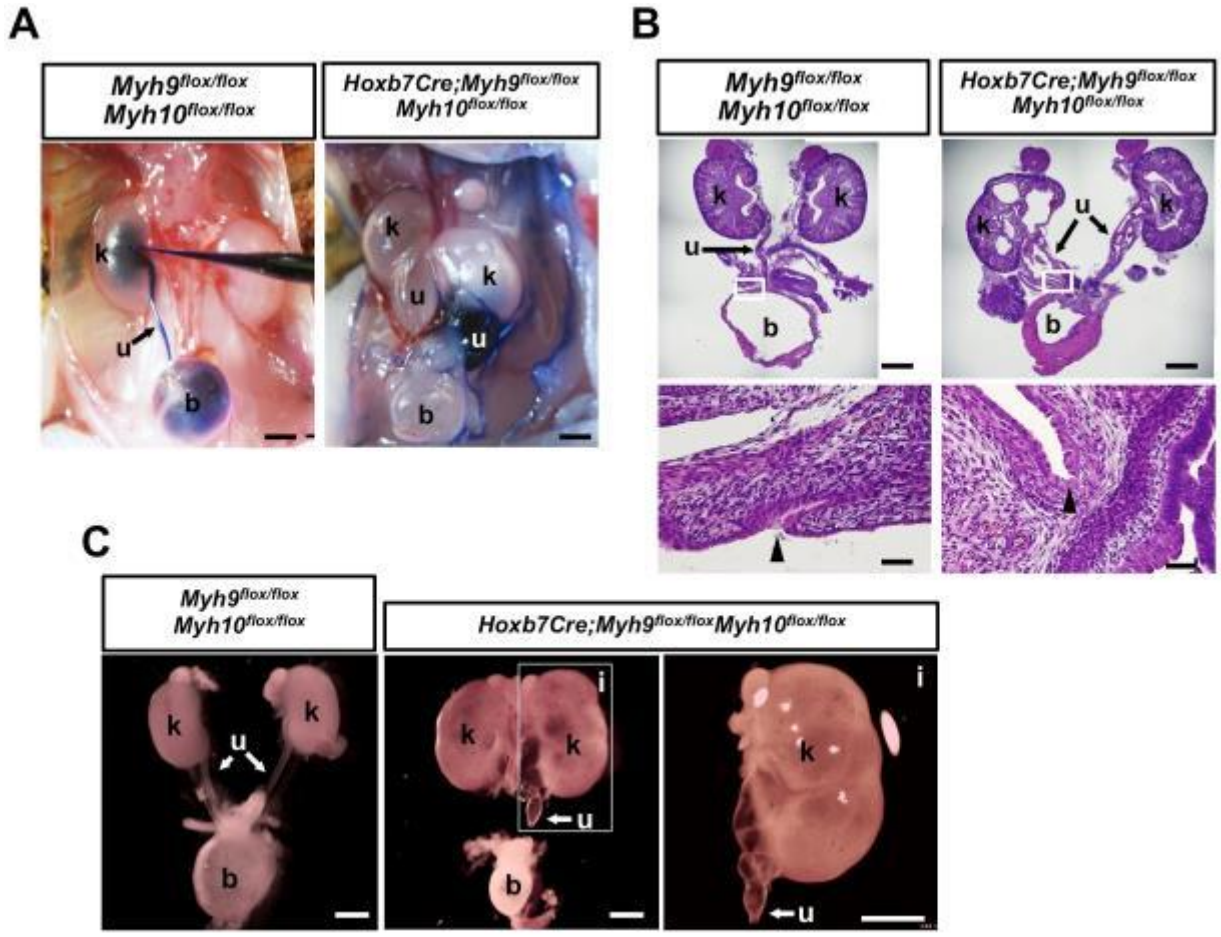

Figure 5: Physical blockade or misconnection between the ureter and bladder causes the hydronephrosis/hydroureter at birth. (A) Ink injected into the renal pelvis flowed through the ureter into the bladder in control mouse, whereas ink was trapped in the ureter and failed to flow into the bladder in mutant mouse (no ink stain). (B) HE staining showed that, while the control ureter opened into the bladder, the mutant ureter lacked a ureter opening (black arrowheads). Second row is magnified views of portions in the first row. (D) Shortened ureters that were completely detached from the bladder in severe cases of Myh9/Myh10 mutant mouse at birth. Both kidneys exhibited hydronephrosis and both ureters were blunt-ended. Scale bars: 1 mm in all panels except for the second row of C (100 μm).

4.5 *Myh9/Myh10* mutant epithelia exhibit ectopic budding, CND malformation, and aberrant basal protrusion at mid-gestation

At E10.5–11.5, the UB sprouts from the ND, and the more caudal part of the ND connected to the cloaca is known as the CND. Subsequently, the CND undergoes physiological apoptosis, leading to a direct connection between the caudal end of the UB (future ureter) and the cloaca (future urinary bladder) (Batourina et al., 2005; Uetani et al., 2009). Thus, it is well established that an abnormal UB budding site at this early developmental stage and malformation of the CND causes misconnection of the ureter and bladder in later development (Mendelsohn, 2009; Stewart and Bouchard, 2014). Various abnormalities were observed in *Myh9/Myh10* double-mutant mice at E11.5 (Figure 6A and 6B). In control kidneys (n = 6), the UB ($Pax2^{+}$/E-$cadherin^{+}$) sprouted from the ND and invaded into the metanephric mesenchyme ($Pax2^{+}$/E-$cadherin^{-}$), while the thick CND was connected to the cloaca ($Pax2^{-}$/E-$cadherin^{+}$). In mutant mice, six of 10 kidneys (60%) were ectopic, and thus multiple, UB formations. The caudal part of the CND, which was in proximity to the cloaca, was apparently narrowed (six kidneys; 60%). This region exhibited physiological apoptosis in control mice, which was significantly reduced in mutant mice (Figure 6C). In addition, tail-like structures were observed in some mutant CNDs (three kidneys; 30%) (Figure 6A). These phenotypes likely represented incomplete CND attachments to the cloaca. Furthermore, it was observed that the mutant ND was barely attached to the cloaca and seemingly passed through the site in one of the E10.5 mutant mice (Figure 6D). Taken together, the mutant kidneys exhibited various degrees of abnormal UB/CND development that subsequently resulted in ureter-bladder misconnection and hydroureter/hydronephrosis.

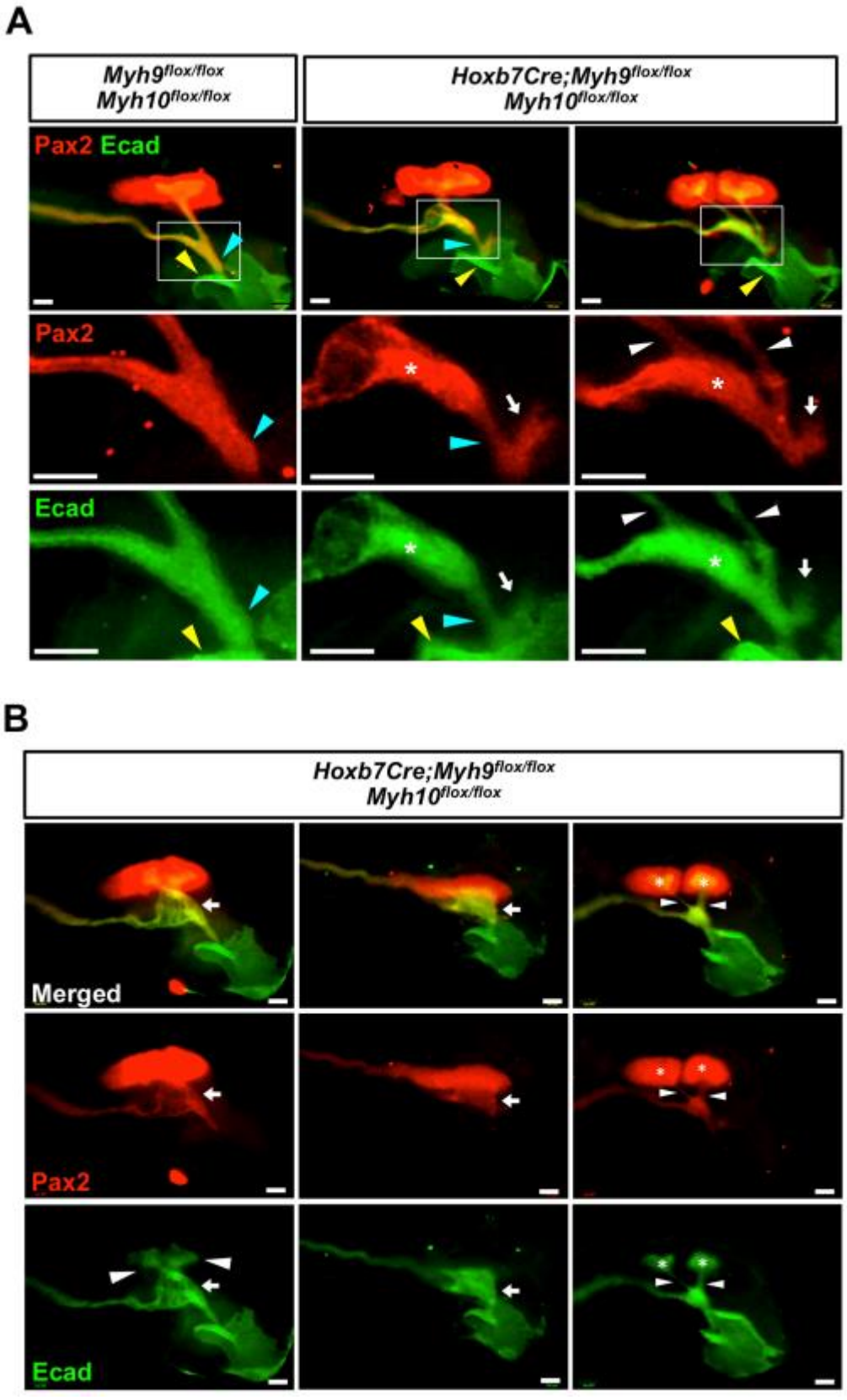
A
Myh9flox/flox
Myh10flox/flox
Hoxb7Cre;Myh9flox/flox
Myh10flox/flox
Pax2 Ecad
Pax2
Ecad
B
Hoxb7Cre;Myh9flox/flox
Myh10flox/flox
Merged
Pax2
Ecad

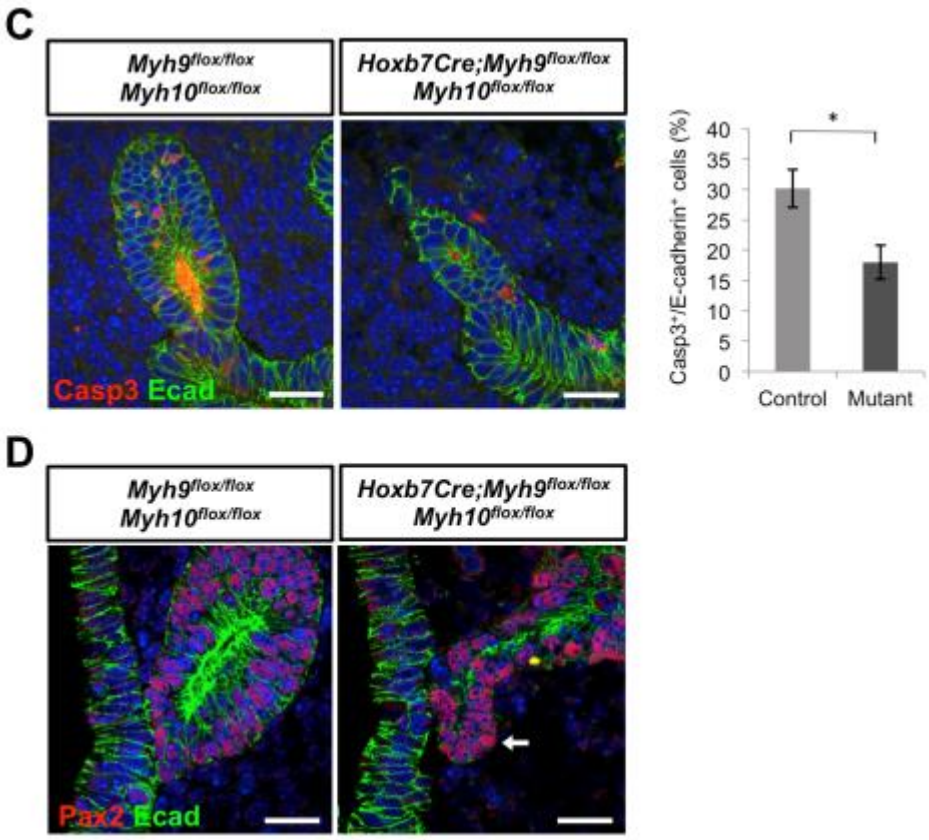

Figure 6: *Myh9/Myh10* mutant epithelia exhibit ectopic budding and various UB/CND abnormalities at mid-gestation. (A and B) Whole mount immunostaining of Pax2/E-cadherin (Ecad) at E11.5. (A) Left panels: control kidneys in which a thick CND ($Pax2^+$/E-$cadherin^+$; cyan arrowheads) was connected to the cloaca ($Pax2^-$/E-$cadherin^+$; yellow arrowheads). Middle and right columns: *Myh9/Myh10* mutant kidneys showed various abnormalities: dilation at ND/UB junctions (asterisks), narrowing of the caudal part of the CND (cyan arrowheads), multiple UBs (white arrowheads), and tail-like structures (white arrows). The second and third rows show magnified views of the first row. (B) Left column: UB/ND junctions were dilated (white arrow), but UB branching was observed (white arrowhead). Middle column: UB/ND junctions were dilated (white arrow) without apparent UB branching. Right column: double UB budding (white arrowheads) from adjacent points of the ND that were also dilated. Two separate kidneys were formed (asterisks). (C) Physiological apoptosis in the narrowed part of the CND in the *Myh9/Myh10* mutant kidney was significantly reduced compared with the control kidney ($p<0.05$). Images show immunostaining of cleaved caspase-3 (Casp3; apoptosis marker) and E-cadherin in E11.5 sections. (D) Section immunostaining of Pax2 (red) and E-cadherin (green) in the CND ($Pax2^+$/E-$cadherin^+$)/cloaca ($Pax2^-$/E-$cadherin^+$) junction at E10.5. While the control CND attached to the cloaca through a wider area (left panel), the *Myh9/Myh10* mutant CND barely attached to the cloaca and appeared to deviate from the site (right panel, white arrow). Scale bars: 100 μm in A, B; 25 μm in C, D.

4.6 *Myh9/Myh10* mutant epithelia exhibit aberrant basal protrusion at mid-gestation

While examining the cause of the abovementioned abnormalities, numerous protrusions from the basal domain of the epithelia were found (Figure 7). In control mice, fibronectin surrounded the basal domain of the epithelia, but it was discontinuous in mutant mice and aligned with the protrusions. Because actomyosin interacts with a fibronectin receptor, integrin (Conti and Adelstein, 2008), the absence of myosin II may affect the activity of integrins located at the cell-basement membrane interface, which would normally maintain the basal integrity of the epithelia. The resultant promiscuous basal protrusions and reduced recognition of the basally contacted epithelia may lead to ectopic UB budding and weaker attachment of the CND to the cloaca, respectively.

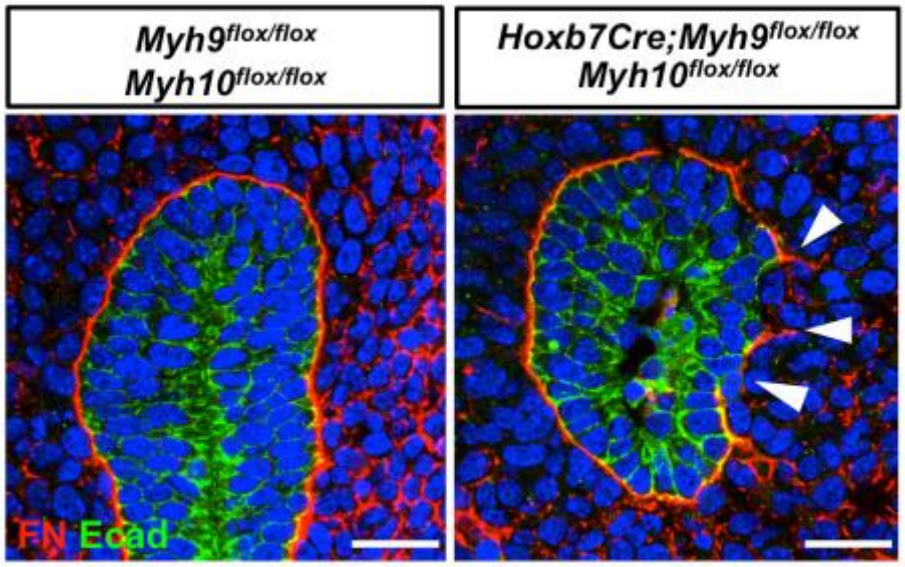

Figure 7: *Myh9/Myh10* mutant epithelia exhibit basal protrusion at mid-gestation. Protrusions from the basal domain of epithelia at E11.5 shown by immunostaining of fibronectin (FN; red) and E-cadherin (Ecad; green). In the control kidney (left panel), the basal domain of the epithelia was surrounded by fibronectin. In the *Myh9/Myh10* mutant kidney (right panel), fibronectin was discontinuous and aligned with the protrusions (white arrowheads). Scale bars: 25 μm.

4.7 *Myh9/Myh10* mutant epithelial cells extrude apically and undergo apoptosis

Another marked abnormality of the mutant mice was dilation of the UB and ND, which was shown to be most prominent at ND/UB junctions by whole mount staining (Figure 6A and 6B). Histological staining of sections confirmed these findings in mutant mice (Figure 8A). In addition, mutant cells in the epithelial layer apically extruded *en masse* into the lumen and underwent massive apoptosis as detected by cleaved caspase-3 staining (Figure 8B).

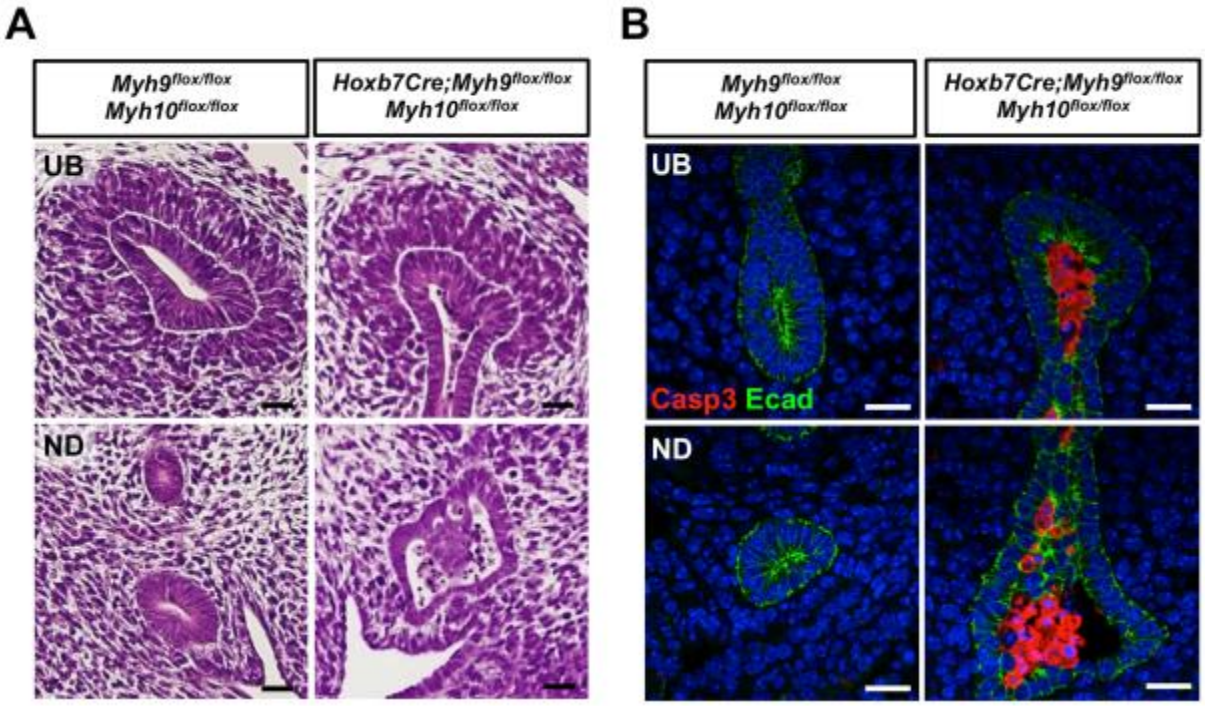

Figure 8: *Myh9/Myh10* mutant epithelial cells extrude apically and undergo apoptosis. (A) HE staining of E11.5 sections showed UB tips and dilated ND with cells extruding *en masse* into the lumen. (B) Immunostaining of cleaved caspase-3 (Casp3; red)/E-cadherin (Ecad; green) in E11.5 sections showed massive apoptosis of cells in the lumen. Scale bars: 25 μm.

It was determined whether the extruding cells were generated by proliferation, but there was no significant difference in the proliferation of the mutant epithelia compared with the control epithelia (Figure 9).

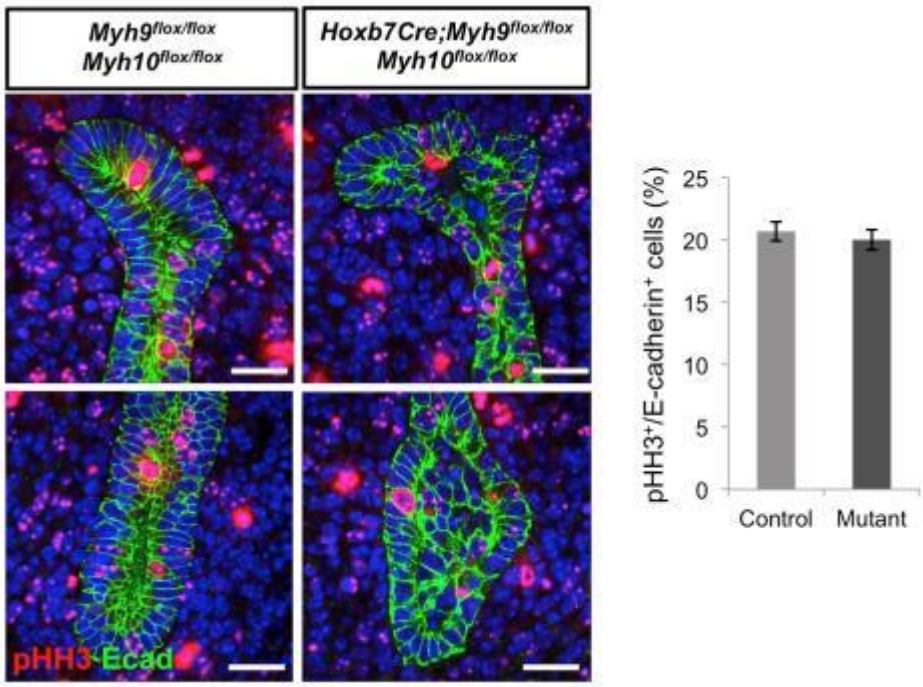

Figure 9: Cell proliferation is unaffected in *Myh9/Myh10* mutants. Immunostaining of mitosis marker pHH3 (red) and E-cadherin (Ecad; green) at E11.5. Left panels: mitotic cells (red) in the UB/ND of control and *Myh9/Myh10* mutant epithelia (green). Right panel: there was no significant difference in the percentages of proliferating cells (pHH3-positive/E-cadherin-positive cells) between control and *Myh9/Myh10* mutant epithelia (p=0.42). Scale bars: 100 μm.

4.8 *Myh9/Myh10* mutant epithelia have reduced intercellular adhesion and apical constriction

While atypical protein kinase C (aPKC) was expressed continuously in the apical domain facing the lumen in control mice, it was discontinuous in mutant mice (Figure 10A and 10B). In control mice, E-cadherin accumulated as dots in most of the apical intercellular

regions, which likely represented adherens junctions, but this accumulation was not evident in some areas of mutant mice, which coincided with the absence of aPKC. In these areas, the width of the apical domain was enlarged compared with the tightly constricted apical domains in control mice (Figure 10A and 10B). These features were observed in mutant cells residing in the epithelial layer or at the forefront of the extruding cell mass (Figure 10A and 10B). Interestingly, the cells inside the extruding mass retained E-cadherin expression, but lacked the apicobasally oriented E-cadherin distribution (Figure 10B). Considering the well-established interaction between actomyosin and E-cadherin at adherens junctions, it can be suggested that the absence of myosin II led to a reduction in E-cadherin-mediated intercellular adhesion and apical constriction, which likely resulted in the apical extrusion. It was also noticed that continuous fibronectin staining was often disrupted in regions where apical extrusion had occurred (Figure 10C), suggesting that the impaired basal attachment may also play a role in the apical extrusion.

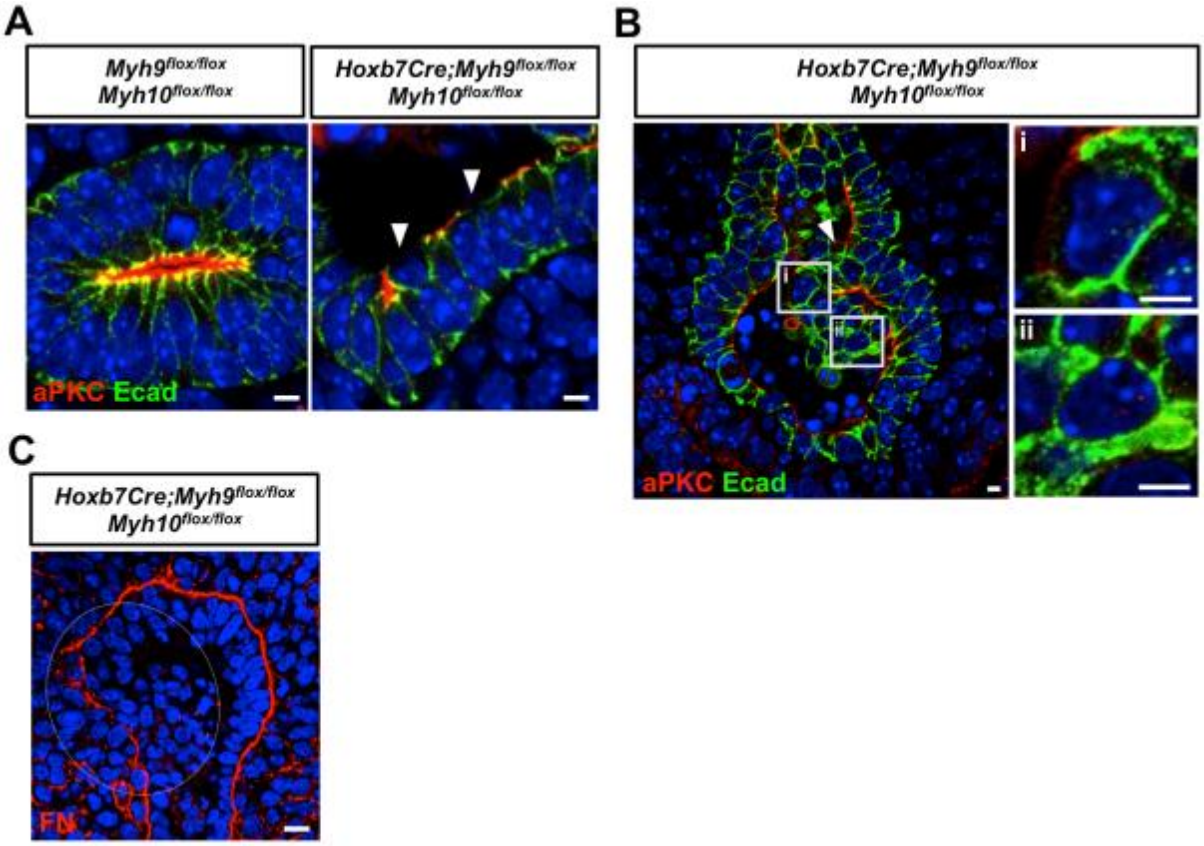

Figure 10: The apical domain in *Myh9/Myh10* mutant epithelia lacks continuous aPKC and E-cadherin accumulation. (A) Immunostaining of aPKC (red; apical marker) and E-cadherin (Ecad; green) in E11.5 sections. Left panel: section from a control mouse. aPKC was continuously expressed in the apical domain facing the lumen. E-cadherin accumulated as dots at apical intracellular regions. Right panel: section from a *Myh9/Myh10* mutant mouse. aPKC expression was not continuous (white arrowheads), dot-like E-cadherin accumulation was not evident at these portions, and the apical domains were widened. (C) Immunostaining of another mutant ND at E11.5. Left panel: aPKC expression was discontinuous (white arrowheads) and cells extruded *en masse* into the lumen. i (magnified portion from left panel): a cell at the forefront of the extruding mass lacked aPKC and dot-like E-cadherin accumulation, and its apical domain was widened. ii (magnified portion from left panel): cells inside the extruding mass retained E-cadherin, but lacked the apicobasally oriented distribution. (C) Discontinuous fibronectin expression (red) in areas where apical extrusion occurred (marked by dashed white line). Scale bars: 5 μm in A, B; 10 μm in C.

4.9 UB dilatation and luminal apoptosis persist at E14.5

UB dilatation and luminal apoptosis, which were observed at E11.5, were persistent at E14.5, a stage before hydronephrosis had occurred (Figure 11).

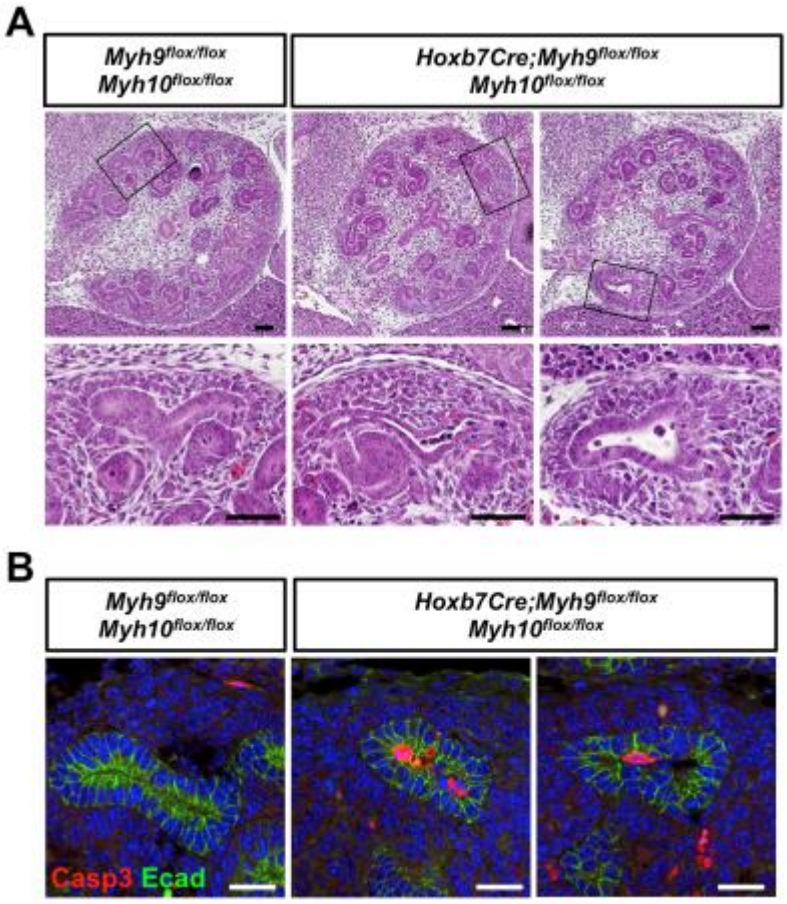

Figure 11: UB dilatation and persistent luminal apoptosis at E14.5. (A) HE staining of control and *Myh10/Myh10* mutant kidneys at E14.5. Dilated UB tips with pyknotic cells were observed in the lumen. (B) Immunostaining of caspase-3 (Casp3; red) and E-cadherin (Ecad; green) at E14.5. Apoptotic cells were detected in the lumen. Scale bars: 100 μm in A; 50 μm in B.

4.10 Phenotypes in *Myh9/Myh10* mutant mice are caused by a Ret-independent mechanism

Ret, which is expressed in the ND/UB, is a critical regulator of UB budding and branching, and Ret hyperactivation leads to ectopic UB budding and subsequent

hydroureter/hydronephrosis (Basson et al., 2005; Grieshammer et al., 2004; Hoshi et al., 2012) resembling the phenotypes of *Myh9/Myh10* mutant mice to some extent. Therefore, I examined the involvement of Ret hyperactivation in *Myh9/Myh10* mutant mice. *Wnt11* and *Ret* itself serve as specific targets in the ND/UB downstream of Ret signaling. *Etv4* functions downstream of *Ret*, although it is also activated in the metanephric mesenchyme downstream of fibroblast growth factor (FGF) signaling. However, *in situ* hybridization of these genes did not show any increased expression in the mutant ND/UB (Figure 12A and 12B). To further examine whether genetic dosage reduction of *Ret* could ameliorate the phenotypes, *Myh9/Myh10*-null/Ret heterozygous mice were generated after crossing *Myh9/Myh10* mutant mice with *Ret* mutant mice. However, the resulting mice showed no significant reduction in the frequencies of hydroureter/hydronephrosis at birth (Figure 12C and 12D). Therefore, based on these data, it can be suggested that the phenotypes in *Myh9/Myh10* mutant mice were unlikely to be caused by Ret hyperactivation. This conclusion was also supported by the fact that narrowing or tail-like structures of the CND as well as ND/UB dilatation and apical extrusion have not been reported in any mice exhibiting a hyperactive state of Gdnf/Ret signaling.

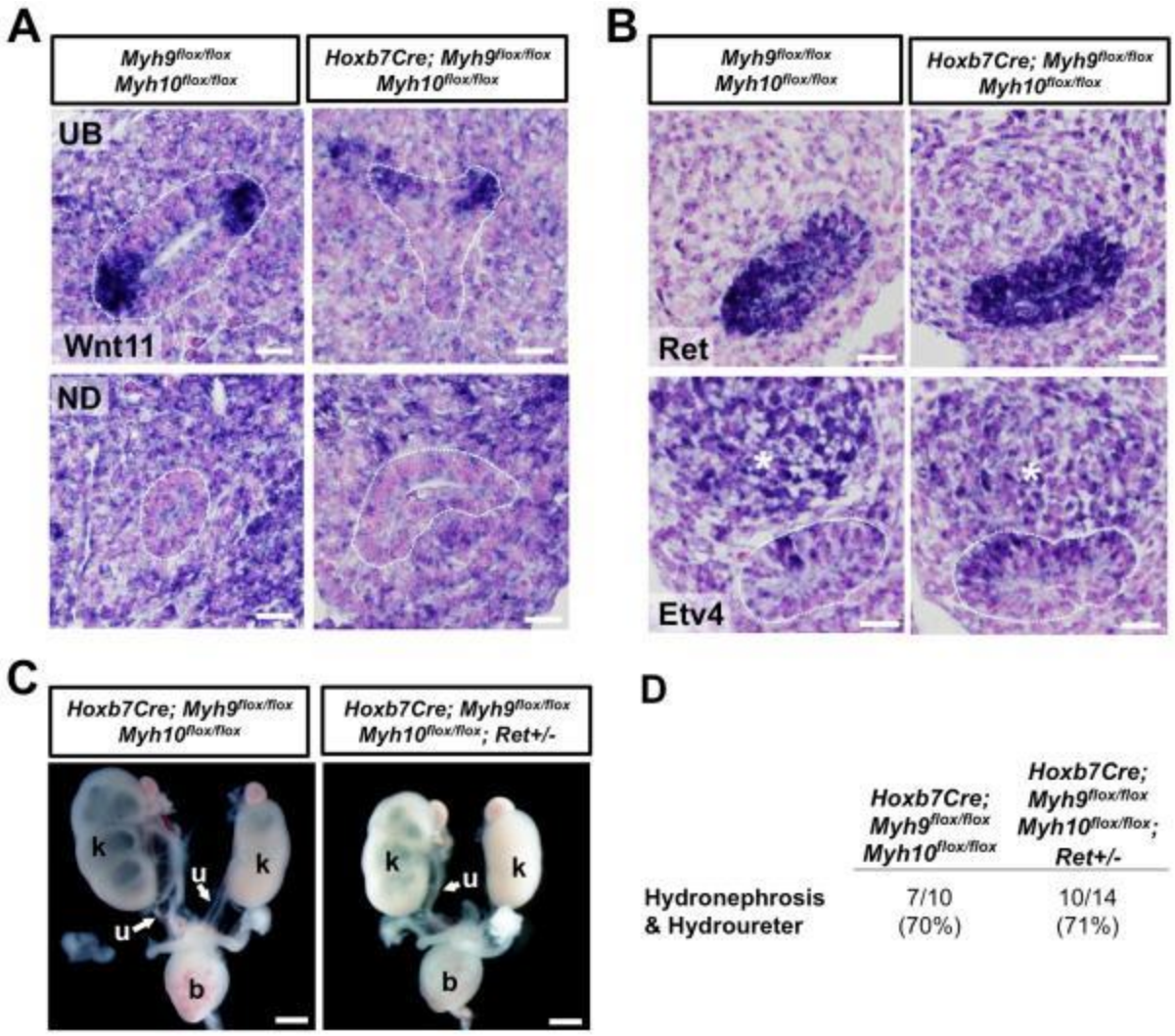

Figure 12: Phenotypes in *Myh9/Myh10* mutant mice are caused by a Ret-independent mechanism. (A) *In situ* hybridization of *Wnt11* in the UB and ND (white dotted lines) at E11.5. *Wnt11* was expressed in the UB tips, but not in the ND, of both control and mutant mice. (B) *In situ* hybridization of Ret and Etv4 in the ND (dotted whites line in right column) at E10.5 showed no difference in expression. Etv4 was also expressed in the metanephric mesenchyme (white asterisks). (C) Both *Myh10/Myh10* mutant mice (left panel) and *Myh9/Myh10*-null/Ret heterozygous mice (right panel) exhibited hydronephrosis/hydroureter at birth. (D) The frequencies of hydronephrosis/hydroureter were similar in *Myh9/Myh10* mutant mice and *Myh9/Myh10*-null/*Ret* heterozygous mice at birth. Scale bars: 50 μm in A, B; 1 mm in C.

Similar phenotypes are observed after ND/UB-specific deletion of *Yap/Taz* (Reginensi et al., 2015). These mutant mice show narrowing and occasionally complete detachment of the CND, as well as tail-like structures of the CND, reportedly resulting from improper ND insertion into the cloaca. UB dilatation and apoptosis were also mentioned in the cited report, but were not described in detail. Because of the similarities in phenotypes, expression of Yap/Taz was examined in *Myh9/Myh10* mutants. However, the expression patterns of Yap/Taz were unaffected, i.e. they were not significantly excluded from nuclei or accumulated in nuclei (Figure 13). These results suggested that, at least, the phenotypes of the *Myh9/Myh10* mutant mice were unlikely to be explained by loss-of-function of Yap/Taz.

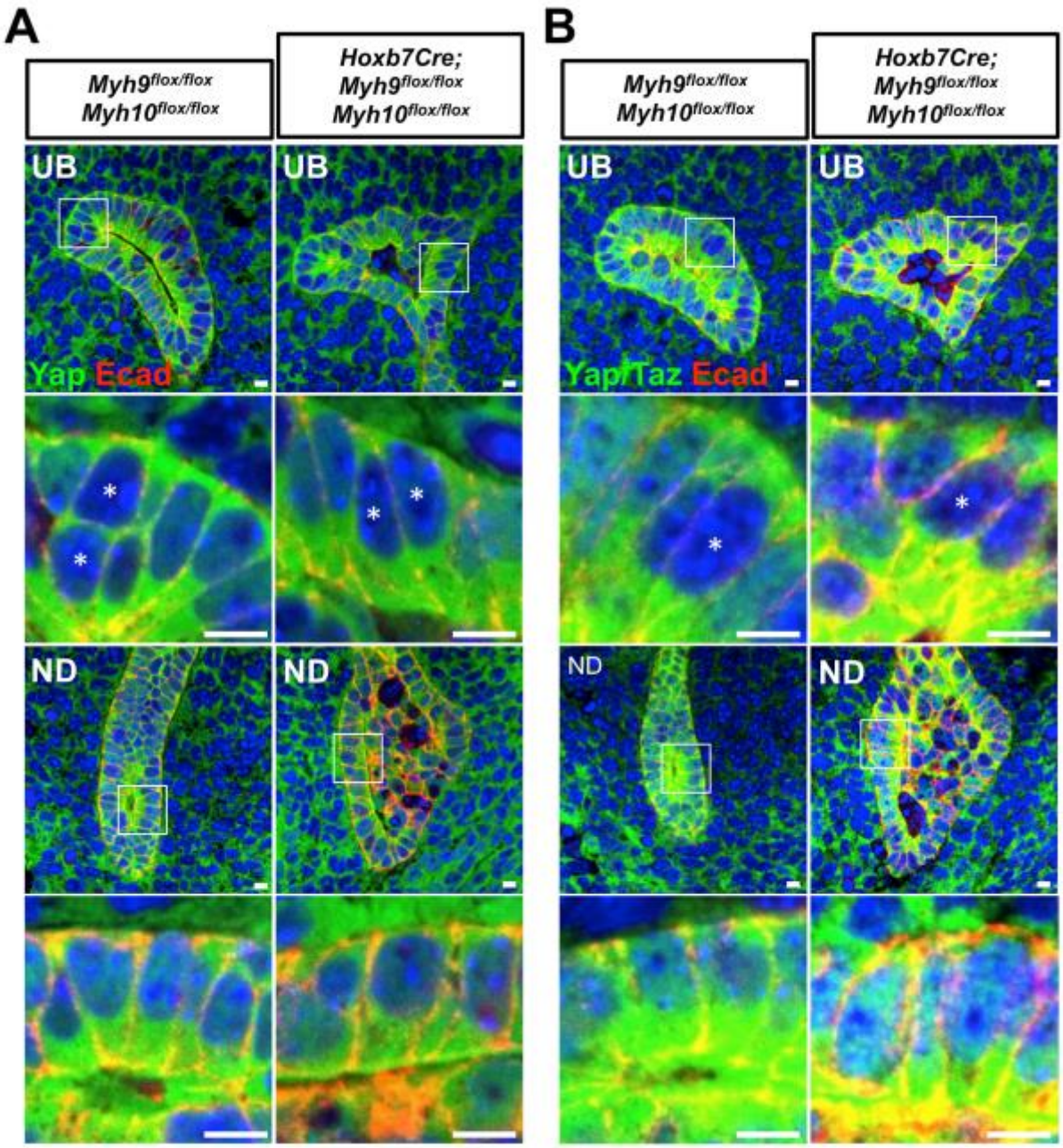

Figure 13: Yap and Yap/Taz show a similar nuclear-cytoplasmic distribution. (A and B) Immunostaining of Yap (A) and Yap/Taz (B) at E11.5. The nuclear-cytoplasmic distribution of Yap and Yap/Taz (green) in E-cadherin^{+} epithelial cells (red) of the UB tip/stalk and ND was not significantly affected in *Myh9/Myh10* mutant mice. Yap and Yap/Taz were distributed ubiquitously in the nuclei and cytoplasm of most cells. A few cells lacked nuclear Yap (asterisks) or Yap/Taz (asterisks), but retained cytoplasmic Yap or Yap/Taz. Second rows in A and B: magnified views of the first rows. Fourth rows in A and B: magnified views of the third rows. Scale bar: 25 μm.

4.11 ERK is hyperactivated in *Myh9/Myh10* mutants

Ret regulates UB budding and branching by activating ERK, and its excessive activation causes ectopic UB budding (Costantini and Kopan, 2010)(Hoshi et al., 2012). Although the above data suggested that Ret was unlikely to be involved in the phenotypes of the *Myh9/Myh10* mutant mouse, it remained possible that ERK activation was involved in the process. Enhanced staining of phosphorylated ERK was observed in mutant mice, in areas where basal protrusion or apical extrusion had occurred (Figure 14A–C). Triple staining revealed that most of the phosphorylated ERK signals were in Myh9-deficient epithelia, indicating that myosin II deficiency led to ERK activation in mutant cells (Figure 14D).

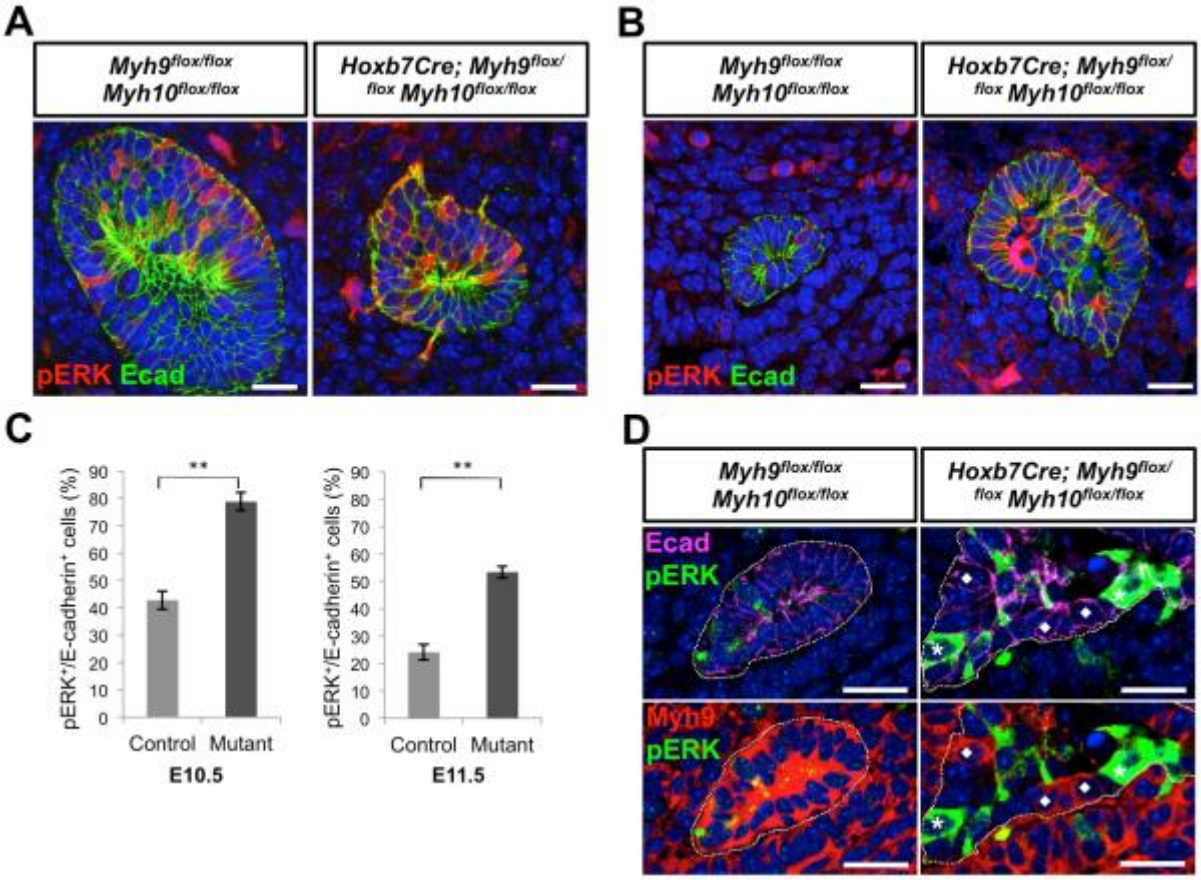

Figure 14: ERK is hyperactivated in *Myh9/Myh10* mutants. (A) Immunostaining of phosphorylated ERK (pERK; red) and E-cadherin (Ecad; green) in the ND at E10.5. ERK was activated in basally protruding cells in the *Myh9/Myh10* mutant mouse. Left panel: control mouse. (B) Immunostaining of pERK (red) and E-cadherin (green) in the ND at E11.5. ERK was activated in apically extruding cells in the mutant mouse (right panel). Left panel: control mouse. (C) Quantitative analysis of $pERK^+$ cells in the ND at E10.5 and E11.5. Significant increases were observed in mutant mice at both stages ($p<0.01$). (D) Triple immunostaining of pERK (green), Myh9 (red), and E-cadherin (magenta) in the ND at E11.5 (dotted white lines). ERK was activated in mutant epithelial cells (white asterisks; right panels), while cells retaining Myh9 did not show ERK activation (diamonds; right panels). Left panels: control mouse. Top and bottom rows show separate images of the same triple-stained sections. Scale bars: 20 μm.

4.12 Inhibition of hyperactivated ERK partially ameliorates the phenotypes

Finally, kidney rudiments isolated at E10.75 were cultured in the presence of the ERK inhibitor U0126. The concentration of U0126 was optimized to show minimal or partial suppression of UB sprouting in wild-type embryos (Figure 15A). While the mutant kidney rudiments showed multiple and dilated UB budding from the ND, the ERK inhibitor suppressed the multiple budding (Figure 15B and 15C). UB dilatation was not ameliorated, probably because the UB was already dilated at the start of the organ culture. Harvesting at earlier developmental stages resulted in variable development of kidney tissues. These results indicated that ERK activation had, at least partially, an important role in causing the mutant mouse phenotypes. Taken together, myosin II deficiency in the ND/UB epithelia had caused Ret-independent ERK activation that possibly led to basal protrusion and apical extrusion, resulting in hydroureter/hydronephrosis and dilation/luminal apoptosis, respectively.

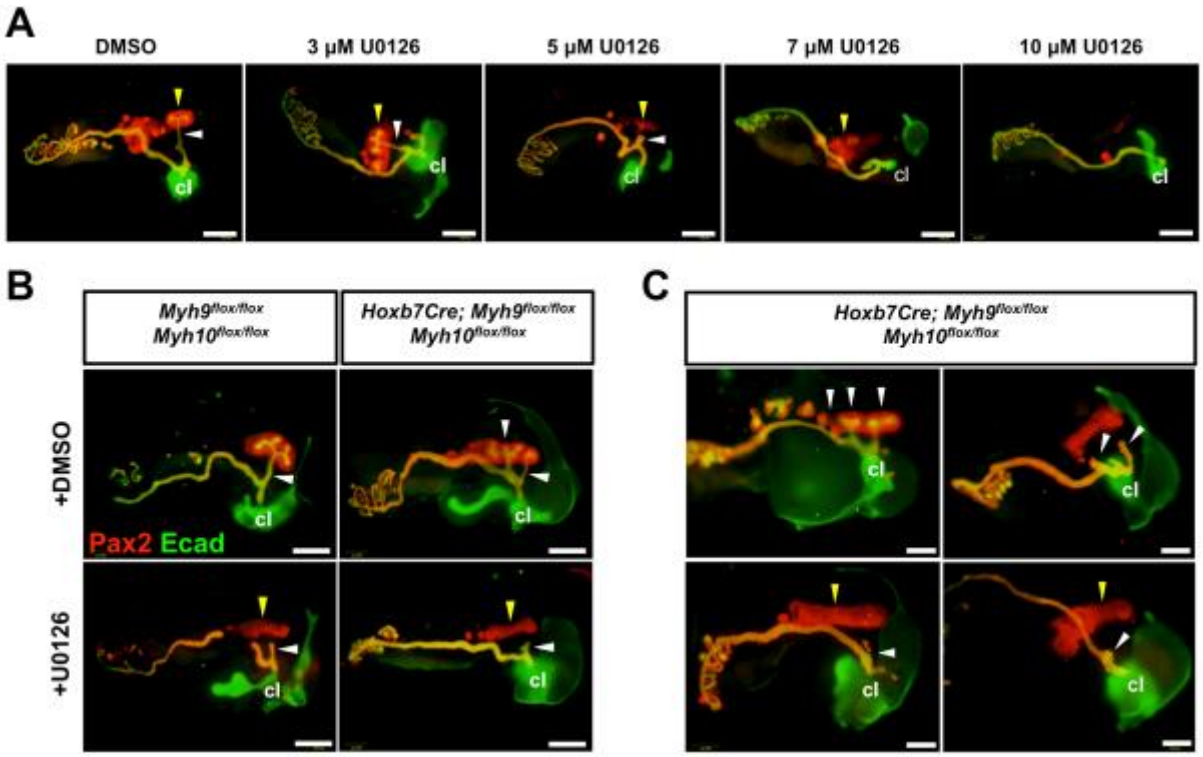

Figure 15: Inhibition of hyperactivated ERK partially ameliorates the phenotypes. (A) Whole mount immunostaining of Pax2 (red) and E-cadherin (green) in kidney rudiments cultured for 48 h starting from E10.75 in the presence of the vehicle (DMSO) or ERK inhibitor U0126 at the indicated concentrations. The images showed minimal suppression of UB budding at 3 μM U0126, but complete suppression of UB budding at 7 and 10 μM U0126. White arrowheads indicate UB budding, and yellow arrowheads indicate metanephric mesenchyme. (B) Whole mount immunostaining of Pax2 (red) and E-cadherin (Ecad; green) in kidney rudiments cultured for 48 h starting from E10.75. First column: wild-type kidney rudiments cultured in DMSO (top row) and in presence of ERK inhibitor U0126 (bottom row). Second column, top row: multiple UB budding (white arrowheads) from the ND in *Myh9/Myh10* mutant kidney rudiments (right panel) cultured in the presence of the vehicle (DMSO). Bottom row: suppressed budding in *Myh9/Myh10* mutant kidney rudiments cultured in the presence of ERK inhibitor U0126. (C) Whole mount immunostaining of Pax2 (red) and E-cadherin (green) in kidney rudiments cultured for 48 h starting from E10.5. Top row: multiple and dilated UB budding (white arrowheads) from the ND in *Myh9/Myh10* mutant kidney rudiments cultured in the presence of the vehicle (DMSO). Bottom row: suppressed budding in *Myh9/Myh10* mutant kidney rudiments cultured in the presence of ERK inhibitor U0126. Yellow arrowheads indicate metanephric mesenchyme. Scale bars: 200 μm.

4.13 Chemical inhibition of myosin II activates ERK in MDCK cells *in vitro*

In MDCK cells, chemical inhibition of myosin by blebbistatin caused ERK activation within 5 min (Figure 16). This result indicated that myosin-mediated adhesion might be involved in excessive ERK suppression, although it may not be necessarily linked to the situation *in vivo*.

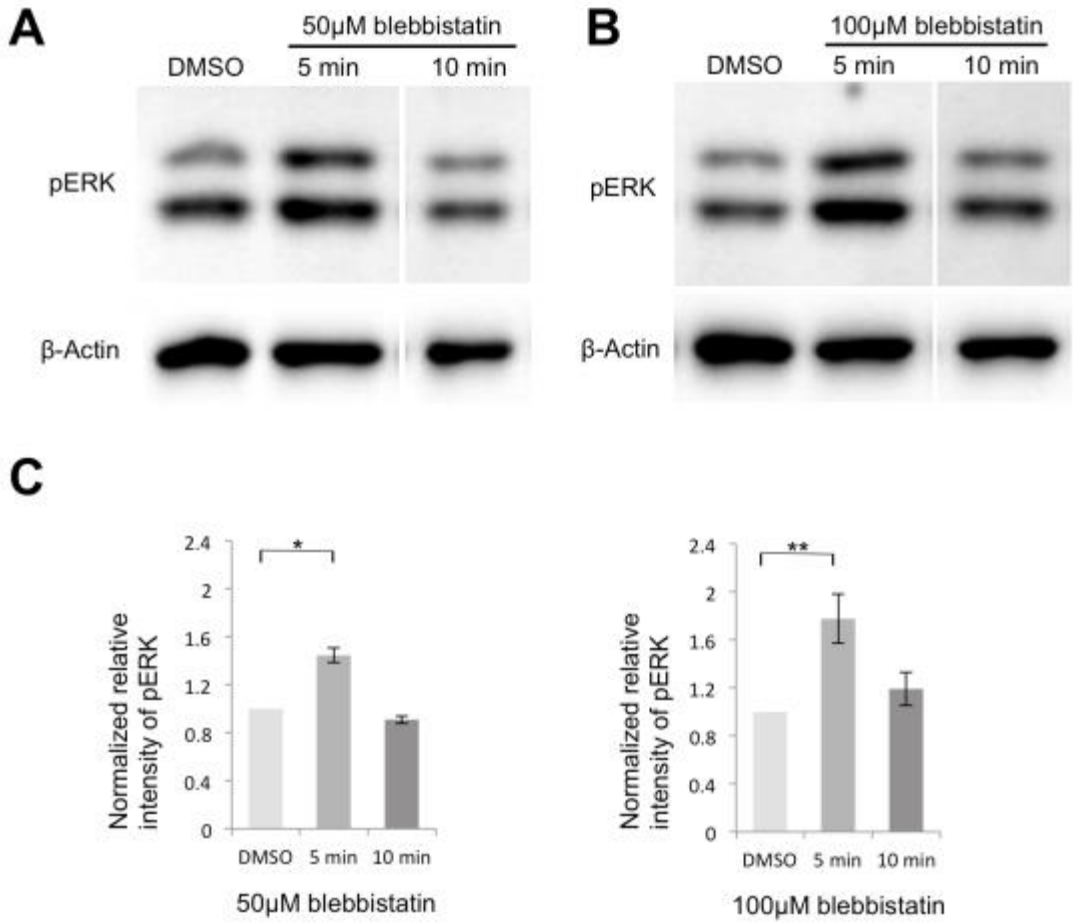

Figure 16: ERK activation in MDCK cells upon blebbistatin treatment. (A and B) MDCK cells were treated with two concentrations of blebbistatin (50 or 100 μM) for 5 or 10 min. At both concentrations, ERK was activated within 5 min of treatment. As a control, MDCK cells were treated with the vehicle (DMSO). The data at 10 min were obtained from distant lanes of the same membranes, and the intervening lanes have been omitted. (C) Quantitative analysis of ERK activation in panels A and B. Data represent the relative intensities of pERK normalized to the intensities of the loading control (β-actin). Significant ERK activation was observed upon blebbistatin treatment for 5 min (*p<0.05; **p<0.01).

5. Discussion

In this study, I have investigated the role of a cytoskeletal protein, non-muscle myosin II (IIA and IIB), in kidney development by specifically deleting the respective NMHC genes in ND/UB lineages of mice. NMHC IIA and IIB, which are encoded by *Myh9* and *Myh10*, respectively, have redundant functions in ND/UB lineages (Recuenco et al., 2014). In this study, it has been shown that non-muscle myosin II is essential for maintenance of epithelial apicobasal integrity, and its deletion leads to promiscuous apical extrusion and basal protrusion, resulting in luminal apoptosis and urinary tract malformation, respectively. In contrast, deletion of myosin II in the metanephric mesenchyme, another essential component of the kidney, does not cause these phenotypes, but affects nascent nephron morphogenesis. Nascent nephrons are shaped irregularly, and impairment of apical constrictions causes discontinuously formed lumen, possibly by preventing the recruitment and integration of the new apical domain into the elongating lumen (Recuenco et al., 2014). In the metanephric mesenchyme, epithelial tubes are newly formed through mesenchymal-to-epithelial transition and subsequently convolute to form nephrons, while epithelial tubes with a pre-existing lumen elongate and branch in ND/UB lineages. These differences in epithelial properties may underlie the distinct roles of myosin II in the two components of the kidney. However, apical constriction is likely to be involved in both types of epithelia, suggesting conservation of at least this role of myosin II. It will be interesting to examine the roles of myosin II in epithelia of other organs. Embryonic lung explants treated with the myosin inhibitor blebbistatin showed an impaired cell shape and arrangement (Plosa et al., 2012), but myosin deletion *in vivo* was not performed. Intestinal epithelium-specific *Myh9*-deficient mice show intestinal barrier disruption, resulting in increased permeability (Naydenov et al., 2016). In these mice, expression of some adherens junction proteins decreases, but the gross morphology is unaffected. Furthermore, *Myh9* deletion in mouse tongue epithelia results in spontaneous squamous cell carcinoma (Conti et al., 2015), the cause of which remains controversial. To the best of my knowledge, deletion of both *Myh9* and *Myh10 in vivo* has not been reported in organ epithelia other than the kidney.

Myosin II is involved in cadherin-mediated intercellular adhesion and apical constriction. It also plays an important role in integrin-mediated adhesion to the basement membrane. The apical extrusion and basal protrusion observed after myosin II deletion suggest that myosin maintains epithelial integrity by preventing the cells from escaping the epithelial layer. Reduced apical intercellular adhesion and a broadened apical domain could

evoke apical extrusion followed by apoptosis, while impaired basal recognition may lead to promiscuous basal protrusion and reduced basal adhesion to the neighboring cloaca epithelia. These phenotypes are rarely observed in other mutant mice in which kidney development is affected.

Ret is a major regulator of ND/UB development, and its excessive activation leads to ectopic UB budding through ERK activation (Hoshi et al., 2012). However, the data suggest that Ret hyperactivation is unlikely to be involved in the phenotypes caused by myosin II deletion. Nevertheless, ERK activation can at least partly explain the phenotypes, based on the chemical inhibition experiments, which showed inhibition of ectopic budding upon culturing myosin mutant kidney rudiments in the presence of the chemical inhibitor. However, it remains unclear how ERK is activated upon myosin II deletion. Inhibition of myosin functions in MDCK cells using the chemical inhibitor blebbistatin led to ERK activation within 5 min. Although this finding may not be directly related to the situation *in vivo*, a mechanism by which myosin-mediated adhesion suppresses excessive ERK activation and contributes to epithelial integrity could exist.

ND/UB-specific deletion of *Yap* and *Yap/Taz* in mice produces marked similarities to the phenotypes of myosin mutant mice, including hydronephrosis and ERK activation (Reginensi et al., 2015). To the best of my knowledge, blind-ended ureters completely detached from the bladder were only observed in *Yap*, *Yap/Taz*, and *Myh9/Myh10* mutant mice among the many mutant mouse strains with impaired UB development. In E11.5 *Yap* or *Yap/Taz* mutant mice, the CND was narrowed or already detached from the cloaca with the former phenotype also observed in *Myh9/Myh10* mutant mice, possibly leading to the later detachment of the ureter from the bladder. It is also noteworthy that metanephric mesenchyme-specific deletion of *Yap/Taz* in mice shows similar phenotypes to those of *Myh9/Myh10* deficiency (morphology defects in nascent nephrons) (Recuenco et al., 2014; Reginensi et al., 2013). Yap/Taz are effectors downstream of tension as well as upstream tension regulators (Low et al., 2014; Porazinski et al., 2015). The unaltered Yap/Taz distribution in the myosin mutant mice suggests that Yap/Taz are not downstream, but possibly upstream of myosin. However, expression of *Etv4*, a Ret activity indicator, is increased in *Yap*-deficient mice and their phenotypes are largely rescued by genetic dosage reduction of *Ret* (Reginensi et al., 2015). Thus, myosin might play a distinct role from Yap/Taz or may have a possible role in Ret-independent molecular events downstream of Yap/Taz. Further studies are needed to clarify the relationships between Yap/Taz and myosin II in kidney epithelia.

Another possible mechanism leading to apical extrusion and basal protrusion is cell competition that occurs when mutant cells are juxtaposed with wild-type cells (Hogan et al., 2009; Igaki et al., 2009; Vaughen and Igaki, 2016). MDCK cells form a two-dimensional monolayer with apicobasal polarity by culture in collagen-coated plates. When MDCK cell lines harboring impaired polarity or activated oncogenic signaling, such as Ras/ERK signaling, are cultured juxtaposed with wild-type cells, they are extruded basally or apically in a non-cell autonomous manner (Hogan et al., 2009; Kajita et al., 2014). Because *Hoxb7Cre* deletes myosin in a mosaic-like manner, cell competition may be involved in the three-dimensional situation *in vivo*. However, evidence for non-cell autonomous effects is required to prove this tempting hypothesis. It can be examined *in vitro* by knocking out *Myh9/Myh10* in MDCK cells in an inducible manner (such as generating an MDCK cell line with tetracycline-inducible *Myh9/Myh10* shRNA) and co-culturing them with wild-type cells.

Finally, *Myh9* mutations cause hereditary kidney diseases in humans (Kelley et al., 2000; Sekine et al., 2010; The May-Hegglin/Fechtner Syndrome Consortium, 2000). Although glomerular abnormalities are their major manifestations, involvement of ND/UB lineages would be worthy of examination in patients. In addition, several groups have recently reported the generation of human kidney tissues from induced pluripotent stem (iPS) cells (Morizane et al., 2015; Taguchi et al., 2014; Takasato et al., 2015). If a complete ND/UB induction protocol can be established, it will enable examination of whether the described phenotypes in the mutant mice are also found in humans using genetically modified iPS cells.

In summary, this study revealed the essential roles of non-muscle myosin II in maintaining renal epithelial integrity (Figure 17). Further studies may provide important information on the complex three-dimensional structures of the kidney as well as human diseases.

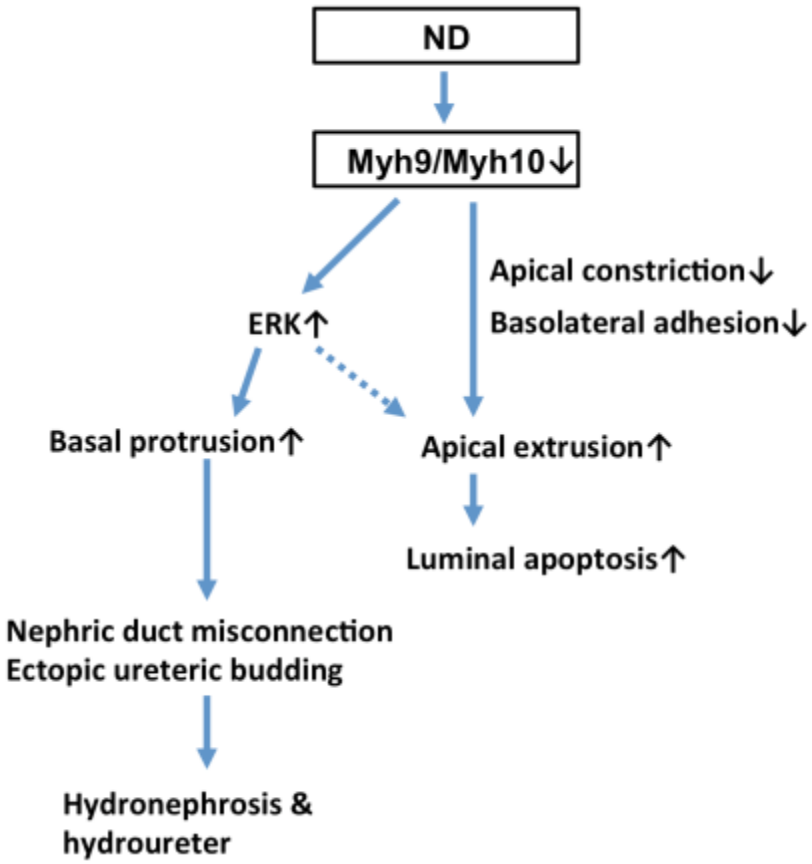

Figure 17: Effects of deleting *Myh9/Myh10* from nephric duct (ND) lineage epithelia.

6. References

Basson, M.A., Akbulut, S., Watson-Johnson, J., Simon, R., Carroll, T.J., Shakya, R., Gross, I., Martin, G.R., Lufkin, T., McMahon, A.P., Wilson, P.D., Costantini, F.D., Mason, I.J., Licht, J.D., 2005. Sprouty1 is a critical regulator of GDNF/RET-mediated kidney induction. Dev Cell 8, 229–239.

Batourina, E., Tsai, S., Lambert, S., Sprenkle, P., Viana, R., Dutta, S., Hensle, T., Wang, F., Niederreither, K., McMahon, A.P., Carroll, T.J., Mendelsohn, C.L., 2005. Apoptosis induced by vitamin A signaling is crucial for connecting the ureters to the bladder. Nat Genet 37, 1082–1089.

Chi, X., Michos, O., Shakya, R., Riccio, P., Enomoto, H., Licht, J.D., Asai, N., Takahashi, M., Ohgami, N., Kato, M., Mendelsohn, C., Costantini, F., 2009. Ret-Dependent Cell Rearrangements in the Wolffian Duct Epithelium Initiate Ureteric Bud Morphogenesis. Dev Cell 17, 199–209.

Conti, M.A., Adelstein, R.S., 2008. Nonmuscle myosin II moves in new directions. J Cell Sci 121,11-18.

Conti, M.A., Even-Ram, S., Liu, C., Yamada, K.M., Adelstein, R.S., 2004. Defects in cell adhesion and the visceral endoderm following ablation of nonmuscle myosin heavy chain II-A in mice. J Biol Chem 279, 41263–41266.

Conti, M.A., Saleh, A.D., Brinster, L.R., Cheng, H., Chen, Z., Cornelius, S., Liu, C., Ma, X., Van Waes, C., Adelstein, R.S., 2015. Conditional deletion of nonmuscle myosin II-A in mouse tongue epithelium results in squamous cell carcinoma. Sci Rep 5, 14068.

Costantini, F., Kopan, R., 2010. Patterning a complex organ: branching morphogenesis and nephron segmentation in kidney development. Dev Cell 18, 698–712.

Durbec, P., Marcos-Gutierrez, C. V, Kilkenny, C., Grigoriou, M., Wartiowaara, K., Suvanto, P., Smith, D., Ponder, B., Costantini, F., Saarma, M., et al., 1996. GDNF signalling through the Ret receptor tyrosine kinase. Nature 381, 789–793.

Grieshammer, U., Ma, L., Plump, A.S., Wang, F., Tessier-Lavigne, M., Martin, G.R., 2004. SLIT2-mediated ROBO2 signaling restricts kidney induction to a single site. Dev Cell 6, 709–717.

Hogan, C., Dupré-Crochet, S., Norman, M., Kajita, M., Zimmermann, C., Pelling, A.E., Piddini, E., Baena-López, L.A., Vincent, J.-P., Itoh, Y., Hosoya, H., Pichaud, F., Fujita, Y., 2009. Characterization of the interface between normal and transformed epithelial cells. Nat Cell Biol 11, 460–467.

Hoshi, M., Batourina, E., Mendelsohn, C., Jain, S., 2012. Novel mechanisms of early upper and lower urinary tract patterning regulated by RetY1015 docking tyrosine in mice. Development 2415, 2405–2415.

Igaki, T., Pastor-Pareja, J.C., Aonuma, H., Miura, M., Xu, T., 2009. Intrinsic Tumor Suppression and Epithelial Maintenance by Endocytic Activation of Eiger/TNF Signaling in Drosophila. Dev Cell 16, 458–465.

Jacobelli, J., Friedman, R.S., Conti, M.A., Lennon-Dumenil, A.-M., Piel, M., Sorensen, C.M., Adelstein, R.S., Krummel, M.F., 2010. Confinement-optimized three-dimensional T cell amoeboid motility is modulated via myosin IIA-regulated adhesions. Nat Immunol 11, 953–961.

Kajita, M., Sugimura, K., Ohoka, A., Burden, J., Suganuma, H., Ikegawa, M., Shimada, T., Kitamura, T., Shindoh, M., Ishikawa, S., Yamamoto, S., Saitoh, S., Yako, Y., Takahashi, R., Okajima, T., Kikuta, J., Maijima, Y., Ishii, M., Tada, M., Fujita, Y., 2014. Filamin acts as a key regulator in epithelial defence against transformed cells. Nat Commun 5, 4428.

Kaku, Y., Ohmori, T., Kudo, K., Fujimura, S., Suzuki, K., Evans, S.M., Kawakami, Y., Nishinakamura, R., 2013. Islet1 Deletion Causes Kidney Agenesis and Hydroureter Resembling CAKUT. J. Am. Soc. Nephrol. 24, 1242–9.

Ke, M.-T., Fujimoto, S., Imai, T., 2013. SeeDB : a simple and morphology-preserving optical clearing agent for neuronal circuit reconstruction. Nat Neurosci 16, 1154–1161.

Kelley, M.J., Jawien, W., Ortel, T.L., Korczak, J.F., 2000. Mutation of MYH9, encoding non-muscle myosin heavy chain A, in May-Hegglin anomaly. Nat Genet 26, 106–108.

Low, B.C., Pan, C.Q., Shivashankar, G. V., Bershadsky, A., Sudol, M., Sheetz, M., 2014. YAP/TAZ as mechanosensors and mechanotransducers in regulating organ size and tumor growth. FEBS Lett. 588, 2663–2670.

Lu, B.C., Cebrian, C., Chi, X., Kuure, S., Kuo, R., Bates, C.M., Arber, S., Hassell, J., MacNeil, L., Hoshi, M., Jain, S., Asai, N., Takahashi, M., Schmidt-Ott, K.M., Barasch, J., D'Agati, V., Costantini, F., 2009. Etv4 and Etv5 are required downstream of GDNF and Ret for kidney branching morphogenesis. Nat. Genet 41, 1295–302.

Majumdar, A., Vainio, S.K.A., Mcmahon, J., Mcmahon, A.P., 2003. Wnt11 and Ret / Gdnf pathways cooperate in regulating ureteric branching during metanephric kidney development. Development 130, 3175–85.

Ma, X., Jana, S.S., Conti, M.A., Kawamoto, S., Claycomb, W.C., Adelstein, R.S., 2010. Ablation of Nonmuscle Myosin II-B and II-C Reveals a Role for Nonmuscle Myosin II in Cardiac Myocyte Karyokinesis. Mol Cell Biol 21, 3952–3962.

Ma, X., Takeda, K., Singh, A., Yu, Z.-X., Zerfas, P., Blount, A., Liu, C., Towbin, J. a, Schneider, M.D., Adelstein, R.S., Wei, Q., 2009. Conditional ablation of nonmuscle myosin II-B delineates heart defects in adult mice. Circ Res 105, 1102–1109.

Mendelsohn, C., 2009. Using mouse models to understand normal and abnormal urogenital tract development. Organogenesis 5, 306–314.

Morizane, R., Lam, A.Q., Freedman, B.S., Kishi, S., Valerius, M.T., Bonventre, J. V, 2015. Nephron organoids derived from human pluripotent stem cells model kidney development and injury. Nat Biotechnol 33, 1193–1200.

Naydenov, N.G., Feygin, A., Wang, D., Kuemmerle, J.F., Harris, G., Conti, M.A., Adelstein, R.S., Ivanov, A.I., 2016. Nonmuscle Myosin IIA Regulates Intestinal Epithelial Barrier in vivo and Plays a Protective Role During Experimental Colitis. Sci Rep 6, 24161. doi:10.1038/srep24161

Pepicelli, C.V., Kispert, A., Rowitch, D.H., and McMahon, A.P. 1997. GDNF induces branching and increased cell proliferation in the ureter of the mouse. Dev. Biol. 192, 193–198.

Plosa, E.J., Gooding, K.A., Zent, R., Prince, L.S., 2012. Nonmuscle myosin II regulation of lung epithelial morphology. Dev Dyn 241, 1770–1781.

Porazinski, S., Wang, H., Asaoka, Y., Behrndt, M., Miyamoto, T., Morita, H., Hata, S., Sasaki, T., Krens, S.F.G., Osada, Y., Asaka, S., Momoi, A., Linton, S., Miesfeld, J.B., Link, B. a., Senga, T., Castillo-Morales, A., Urrutia, A.O., Shimizu, N., Nagase, H., Matsuura, S., Bagby, S., Kondoh, H., Nishina, H., Heisenberg, C.-P., Furutani-Seiki, M., 2015. YAP is essential for tissue tension to ensure vertebrate 3D body shape. Nature 521, 217–221.

Recuenco, M.C., Ohmori, T., Tanigawa, S., Taguchi, A., Fujimura, S., Conti, M. a., Wei, Q., Kiyonari, H., Abe, T., Adelstein, R.S., Nishinakamura, R., 2014. Nonmuscle Myosin II Regulates the Morphogenesis of Metanephric Mesenchyme-Derived Immature Nephrons. J Am Soc Nephrol 26, 1081–1091.

Reginensi, A., Hoshi, M., Boualia, S.K., Bouchard, M., Jain, S., McNeill, H., 2015. Yap and Taz are required for Ret-dependent urinary tract morphogenesis. Development 142, 2696–2703.

Reginensi, A., Scott, R.P., Gregorieff, A., Bagherie-Lachidan, M., Chung, C., Lim, D.-S., Pawson, T., Wrana, J., McNeill, H., 2013. Yap- and Cdc42-dependent nephrogenesis and morphogenesis during mouse kidney development. PLoS Genet 9, e1003380.

Schneider, C. A, Rasband, W.S., Eliceiri, K.W., 2012. NIH Image to ImageJ: 25 years of image analysis. Nat Methods 9, 671–675.

Sekine, T., Konno, M., Sasaki, S., Moritani, S., Miura, T., Wong, W., Nishio, H., Nishiguchi, T., Ohuchi, M.Y., Tsuchiya, S., Matsuyama, T., Kanegane, H., Ida, K., Miura, K., Harita, Y., Hattori, M., Horita, S., Igarashi, T., Saito, H., Kunishima, S., 2010. Patients with Epstein-Fechtner syndromes owing to MYH9 R702 mutations develop progressive proteinuric renal disease. Kidney Int 78, 207–214.

Short, K.M., Smyth, I.M., 2016. The contribution of branching morphogenesis to kidney development and disease. Net Rev Neph 12, 754-767.

Smutny, M., Cox, H.L., Leerberg, J.M., Kovacs, E.M., Conti, M.A., Ferguson, C., Hamilton, N. a, Parton, R.G., Adelstein, R.S., Yap, A.S., 2010. Myosin II isoforms identify distinct functional modules that support integrity of the epithelial zonula adherens. Nat Cell Biol 12, 696–702.

Stewart, K., Bouchard, M., 2014. Coordinated cell behaviours in early urogenital system morphogenesis. Semin Cell Dev Biol 36, 13–20.

Taguchi, A., Kaku, Y., Ohmori, T., Sharmin, S., Ogawa, M., Sasaki, H., Nishinakamura, R., 2014. Redefining the in vivo origin of metanephric nephron progenitors enables generation of complex kidney structures from pluripotent stem cells. Cell Stem Cell 14, 53–67.

Takasato, M., Er, P.X., Chiu, H.S., Maier, B., Baillie, G.J., Ferguson, C., Parton, R.G., Wolvetang, E.J., Roost, M.S., Chuva de Sousa Lopes, S.M., Little, M.H., 2015. Kidney

organoids from human iPS cells contain multiple lineages and model human nephrogenesis. Nature 526, 564–568.

Tanigawa, S., Sharma, N., Hall, M.D., Nishinakamura, R., Perantoni, A.O., 2015. Preferential Propagation of Competent SIX2+ Nephronic Progenitors by LIF/ROCKi Treatment of the Metanephric Mesenchyme. Stem Cell Reports 5, 435–447.

The May-Hegglin/Fechtner Syndrome Consortium, 2000. Mutations in MYH9 result in the May-Hegglin anomaly , and Fechtner and Sebastian syndromes. Nat Genet 26, 103–105.

Tullio, A.N., Accili, D., Ferrans, V.J., Yu, Z.X., Takeda, K., Grinberg, A., Westphal, H., Preston, Y. a, Adelstein, R.S., 1997. Nonmuscle myosin II-B is required for normal development of the mouse heart. Proc Natl Acad Sci USA 94, 12407–12412.

Uesaka, T., Nagashimada, M., Enomoto, H., 2013. GDNF signaling levels control migration and neuronal differentiation of enteric ganglion precursors. J Neurosci 33, 16372–16382.

Uetani, N., Bertozzi, K., Chagnon, M.J., Hendriks, W., Tremblay, M.L., Bouchard, M., 2009. Maturation of ureter-bladder connection in mice is controlled by LAR family receptor protein tyrosine phosphatases. J Clin Invest 119, 924–935.

Vaughen, J., Igaki, T., 2016. Slit-Robo Repulsive Signaling Extrudes Tumorigenic Cells from Epithelia. Dev Cell 39, 683–695.

Yu, J., Carroll, T.J., McMahon, A.P., 2002. Sonic hedgehog regulates proliferation and differentiation of mesenchymal cells in the mouse metanephric kidney. Development 129, 5301–5312.